Atmos. Chem. Phys. Discuss., 11, 745–812, 2011
www.atmos-chem-phys-discuss.net/11/745/2011/
doi:10.5194/acpd-11-745-2011

Atmospheric Chemistry and Physics Discussions

In-situ measurements of tropical cloud properties in the West African monsoon: upper tropospheric ice clouds, mesoscale convective system outflow, and subvisual cirrus

W. Frey[1], S. Borrmann[1,2], D. Kunkel[1], R. Weigel[2], M. de Reus[3], H. Schlager[4], A. Roiger[4], C. Voigt[2,4], P. Hoor[2], J. Curtius[5], M. Krämer[6], C. Schiller[6], C. M. Volk[7], C. D. Homan[7,*], F. Fierli[8], G. Di Donfrancesco[9], A. Ulanovsky[10], F. Ravegnani[8], N. M. Sitnikov[10], S. Viciani[11], F. D'Amato[11], G. N. Shur[10], G. V. Belyaev[12], K. S. Law[13], and F. Cairo[8]

[1]Max Planck Institute for Chemistry, Particle Chemistry Department, Mainz, Germany
[2]Institute for Atmospheric Physics, Johannes-Gutenberg University, Mainz, Germany
[3]Elementar Analysensysteme GmbH, Hanau, Germany
[4]Institut für Physik der Atmosphäre, DLR, Oberpfaffenhofen, Germany

[5]Institute for Atmospheric and Environmental Sciences, Frankfurt University, Frankfurt, Germany
[6]Forschungszentrum Jülich, IEK-7, Jülich, Germany
[7]Department of Physics, University of Wuppertal, Germany
[8]Institute of Atmospheric Science and Climate, ISAC-CNR, Rome, Italy
[9]Ente Nazionale per le Nuove tecnologie, l'Energia e l'Ambiente, Frascati, Italy
[10]Central Aerological Observatory, Dolgoprudny, Moskow Region, Russia
[11]CNR-INO National Institute of Optics, Florence, Italy
[12]MDB-Myasishchev Design Bureau, Zhukovsky-5, Moscow Region, Russia
[13]UPMC Univ. Paris 06, Université Versailles St.-Quentin, CNRS/INSU, LATMOS-IPSL, Paris, France
[*]now at: KNMI, De Bilt, The Netherlands

Received: 3 December 2010 – Accepted: 22 December 2010 – Published: 10 January 2011

Correspondence to: S. Borrmann (stephan.borrmann@mpic.de)

Published by Copernicus Publications on behalf of the European Geosciences Union.

Abstract

In-situ measurements of ice crystal size distributions in tropical upper troposphere/lower stratosphere (UT/LS) clouds were performed during the SCOUT-AMMA campaign over West Africa in August 2006. The cloud properties were measured with a Forward Scattering Spectrometer Probe (FSSP-100) and a Cloud Imaging Probe (CIP) operated aboard the Russian high altitude research aircraft M-55 "Geophysica" with the mission base in Ouagadougou, Burkina Faso. A total of 117 ice particle size distributions were obtained from the measurements in the vicinity of Mesoscale Convective Systems (MCS). Two or three modal lognormal size distributions were fitted to the average size distributions for different potential temperature bins. The measurements showed proportionate more large ice particles compared to former measurements above maritime regions. With the help of trace gas measurements of NO, NO_y, CO_2, CO, and O_3, and satellite images clouds in young and aged MCS outflow were identified. These events were observed at altitudes of 11.0 km to 14.2 km corresponding to potential temperature levels of 346 K to 356 K. In a young outflow (developing MCS) ice crystal number concentrations of up to 8.3 cm^{-3} and rimed ice particles with maximum dimensions exceeding 1.5 mm were found. A maximum ice water content of 0.05 $g\,m^{-3}$ was observed and an effective radius of about 90 µm. In contrast the aged outflow events were more diluted and showed a maximum number concentration of 0.03 cm^{-3}, an ice water content of 2.3×10^{-4} $g\,m^{-3}$, an effective radius of about 18 µm, while the largest particles had a maximum dimension of 61 µm.

Close to the tropopause subvisual cirrus were encountered four times at altitudes of 15 km to 16.4 km. The mean ice particle number concentration of these encounters was 0.01 cm^{-3} with maximum particle sizes of 130 µm, and the mean ice water content was about 1.4×10^{-4} $g\,m^{-3}$. All known in-situ measurements of subvisual tropopause cirrus are compared and an exponential fit on the size distributions is established in order to give a parameterisation for modelling.

ACPD

11, 745–812, 2011

Tropical ice clouds: MCS outflow, anvil, and subvisual cirrus

W. Frey et al.

A comparison of aerosol to ice crystal number concentrations, in order to obtain an estimate on how many ice particles result from activation of the present aerosol, yielded low activation ratios for the subvisual cirrus cases of roughly one cloud particle per 30 000 aerosol particles, while for the MCS outflow cases this resulted in a high ratio of one cloud particle per 300 aerosol particles.

1 Introduction

Tropical convective clouds and Mesoscale Convective Systems (MCS) are key elements of the hydrological cycle, the exchange of air masses between troposphere and stratosphere (Pommereau, 2010), the global circulation (Houze, 2004; Schumacher et al., 2004), and with this, key elements of the global climate. As large, organised, multi-cell systems of cumulonimbus (Cb) clouds the MCS (i.e., Mesoscale Convective Complexes (MCC) or squall lines) belong to the most intense thunderstorms worldwide (Fritsch and Forbes, 2001; Zipser et al., 2006). The area which is covered by MCS cold cloud shields can reach 1 000 000 km^2 while in the global mean they mostly exhibit sizes between 200 000 and 400 000 km^2 (Laing and Fritsch, 1997). Their precipitation regions can have dimensions larger than 1000 km in one direction and produce most of the tropical rainfall. The uppermost parts of MCSs consist of large anvils and surrounding cold cloud shields as cirrus decks which can produce detached fields of upper tropospheric cirrus and subvisual cirrus (Houze, 2004; Thomas et al., 2002). Both kinds of ice clouds influence the Earth's radiative budget (Ackerman et al., 1988; Davis et al., 2010, and references therein). Also MCSs vertically redistribute latent heat and provide fast pathways for upward transport of air from the boundary layer to the upper troposphere/lower stratosphere (UT/LS). Of particular interest in this context are the West African MCSs which occur during the monsoon wet season in the months of July and August with an average frequency near 86 per season (Barnes, 2001; Protat et al., 2010).

ACPD
11, 745–812, 2011

Based on observations in 1986 and 1987 West African MCSs are found to have an average lifetime of 11.5 h, form in the evening near 21:00 local time (LT), reach their maximum extent around 02:00 LT, and dissipate in the mornings near 08:30 LT (Barnes, 2001). Between pressure altitude levels from 700 hPa to 100 hPa West African MCSs have significantly higher buoyancy than those over the Maritime Continent (i.e. Southeast Asia) or the Bay of Bengal. The reasons are inherent in the different vertical free atmosphere temperature profiles: These are dry adiabatic over West Africa and moist adiabatic over the Maritime Continent (Cetrone and Houze, 2009). As consequence convection might be deeper over West Africa and the resulting strong updraughts produce stronger precipitation events with larger hydrometeors. This is suggested by analysis of radar data from the Tropical Rainfall Measuring Mission (TRMM) satellite by Cetrone and Houze (2009). Another consequence is that MCSs frequently extend to altitudes above ≈14 km and penetrate the bottom layer of the Tropical Transition Layer (TTL; as defined by Park et al., 2007). The MCS outflows typically occur at altitudes between 12 km and 16 km and detrain trace gases and aerosols or ozone precursor gases (Homan et al., 2010; Fierli et al., 2010) into the TTL. Such processes significantly influence the aerosol and water content of the TTL (Fueglistaler et al., 2009), as well as the chemical composition of the air within the UT/LS (Huntrieser et al., 2009; Barret et al., 2010). For example, overshooting Cb can penetrate into the stratosphere (Khaykin et al., 2009) and directly deposit ice crystals, aerosols and trace gases (De Reus et al., 2009; Corti et al., 2008). Mesoscale model simulations together with in situ observations of various trace gases lead to the conclusion that detrainment residues from deep convection of MCS can be found at altitudes as high as 17 km (Fierli et al., 2010). Within the TTL air masses carried aloft from the boundary layer by local deep convection encounters air transported into the region from long distances. Domain filling trajectory analyses of air mass origins for the West African TTL of August 2006 indicate that roughly 39% of the air masses below 370 K were influenced by lower tropospheric air from Asia, India, and oceanic regions (Law et al., 2010). Those air masses might concomitantly be influenced by local convection over West Africa. In the lower TTL

ACPD
11, 745–812, 2011

here, Law et al. (2010) estimated that about 50% of the air masses were affected by local convection. Mixing within the TTL occurs because the residence time of air here can be of the order of weeks (Plöger et al., 2010; Krüger et al., 2009). For the case of the 2006 West African monsoon wet season in situ CO_2 measurements showed that convective outflow imported boundary layer air into the TTL between 350 K and 370 K potential temperature levels (Homan et al., 2010) while simultaneous presence of more aged air was demonstrated by means of ozone data. Lightning produces NO_x and thus, enhanced levels of NO and NO_y (Schumann and Huntrieser, 2007; Huntrieser et al., 2009) can be detected inside the MCS outflows. Similarly, trace gases like CO and CO_2 from biomass burning and boundary layer air can be used to identify outflows. Occasionally, a fraction of the SO_2 entering a Cb from the boundary layer also reaches the outflow region (Barth et al., 2007, 2001). The high radiation levels lead to enhanced OH radical production and fast oxidation of the SO_2 to H_2SO_4 which can trigger new particle formation events inside outflow air (Weigel et al., 2011) and even inside clouds (Lee et al., 2004). Thus, the Cb outflows constitute a source for ultrafine particles and it has been speculated that this affects the chemical particle composition in the lower TTL (Borrmann et al., 2010; Weigel et al., 2011). Therefore, besides ground based, remote sensing and satellite data, in-situ measurements within MCS outflows and the involved MCS cloud parts are important for the characterisation of the TTL air. The same is true for the tropical cirrus. This is of relevance since parts of the TTL air ultimately are lifted into the stratosphere and globally distributed. However, direct investigations on the microphysical properties of the MCS upper cloud parts are difficult and rare in general and in particular over West Africa.

Subvisual cirrus (SVC) clouds within the TTL have been frequently detected by satellite platforms (e.g., Winker and Trepte, 1998; Wang et al., 1996; Sassen et al., 2009) and occasionally probed by in-situ measurements (e.g., McFarquhar et al., 2000; Thomas et al., 2002; Lawson et al., 2008; Davis et al., 2010; Froyd et al., 2010). Although optically thin these clouds are believed to influence the radiative transfer because of their large horizontal extent (McFarquhar et al., 2000; Davis et al., 2010).

ACPD
11, 745–812, 2011

Furthermore, they play a major role in the context of freeze-drying air ascending in the tropics towards the stratosphere (Jensen et al., 1996, 2001; Luo et al., 2003a; Peter et al., 2003).

The formation of large horizontal sheets of SVCs disconnected and far away from convective clouds in clear sky (like observed by Winker and Trepte, 1998) probably is a result of deposition freezing. Furthermore, it is dependent on the properties of the nucleating aerosol because these clouds originate from synoptic scale slow uplift (Jensen et al., 1996). The exact mechanisms leading to nucleation and cloud formation in the TTL still are unknown (Froyd et al., 2009). For example Froyd et al. (2010) concluded from air-borne mass spectrometric composition measurements of ice residues in Middle American SVCs that most residuals were internal mixtures of neutralised sulphate and some organics. Mineral dust or other heterogeneous nuclei were not major components. Other field and laboratory studies, however, show the importance of metals (Cziczo et al., 2009, and references therein), mineral dust (DeMott et al., 2003; Zimmermann et al., 2008; Kulkarni and Dobbie, 2010), and organics (Murray et al., 2010) for ice formation. Model calculations by Kärcher (2002) demonstrated that homogeneous freezing of supercooled aerosols could occur at temperatures near 215 K at vertical updraughts of 1 cm s^{-1} to 2 cm s^{-1} and result in ice particle number concentrations of up to 0.1 cm^{-3}. Another conclusion of Kärcher (2002) (and also from Kärcher, 2004) is that heterogeneous freezing from ice nuclei at concentrations below 0.1 cm^{-3} could initiate and control SVC formation at temperatures below the threshold for homogeneous freezing even if the homogeneous freezing nuclei are available at higher concentrations than deposition freezing nuclei. Jensen et al. (2008) performed model simulations on the question how ice crystals as large as 100 µm can form at the tropopause. Based on these simulations water vapour mixing ratios of at least 2 µmol/mol and steady vertical speeds of 2 cm s^{-1} are needed to levitate such particles in the TTL. The model calculations also indicate that homogeneous freezing would result in ice particle concentrations which are too high to obtain closure between the large crystal sizes and the given water vapour abundance. Thus, they conclude that heterogeneous freezing occurred for the analysed cases on effective deposition freezing nuclei at low supersaturations with respect to ice. Also, the importance of fluctuations in temperature and vertical wind velocities for the formation and maintenance of subvisual or opaque cirrus has been pointed out by Jensen et al. (2001, 2010) and for mid latitude cirrus by Haag and Kärcher (2004).

A stabilisation mechanism for the maintenance of SVC consisting of small particles (<20 µm) at the tropical tropopause over long times and large horizontal areas has been suggested by Luo et al. (2003b). According to their hypothesis a slightly supersaturated layer of air lies directly above a slightly subsaturated layer. Both layers are adjacent and below the tropopause in a region where air slowly rises through them driven by large scale ascent (e.g., induced by the Hadley cell). Ice particles in the size range of 10 µm partially evaporate in the subsaturated layer, shrink in size, and ascend carried by the flow into the supersaturated zone aloft. There, they grow again, attain too much mass and fall back down into the subsaturated layer below where they start evaporating again. The according model calculations by Luo et al. (2003b) were based on the measurements of Thomas et al. (2002) from APE-THESEO campaign (Stefanutti et al., 2004) over the Seychelles in 1999. The model showed that such a scenario yields a consistent picture in terms of the small particle sizes and number densities observed there, if the vertical wind speeds are in the range of a few mm/s. This model, however, fails for the large SVC particles observed by Lawson et al. (2008) and Davis et al. (2010), and the data presented in this paper from West Africa.

In the vicinity of individual MCS the occurrence of SVC has been observed for example by Thomas et al. (2002). Here, and in particular under the inhomogeneous conditions as prevailing in large fields of MCSs during the West African Monsoon period, a combination of mechanisms may be responsible for cirrus formation and maintenance. Ice particles could result from homogeneous freezing inside the cumulonimbus clouds and detrain in Cb outflows. External versus internal mixtures of heterogeneous ice nuclei may play a role (also for homogeneous freezing) as the influence of size dependent freezing thresholds does (Spichtinger and Cziczo, 2010). The possibility

ACPD
11, 745–812, 2011

of gravity wave induced shear off of thin cirrus sheets from large Cb anvils exists like Wang (2003) demonstrated for mid latitude Cb. Since such ice cloud sheets would occur below or at the bottom of the TTL additional lofting would be necessary. As discussed in Corti et al. (2006) for tropical troposphere-stratosphere exchange such upwelling may occur here, too, by cirrus cloud-radiation interaction in the vicinity of recent deep convection.

From this brief discussion it becomes clear that many open questions remain in the context of tropical SVC and MCSs in particular over the African continent.

Here, we present in-situ measurements of the tropical UT/LS from the SCOUT-AMMA campaign (Cairo et al., 2010b) in Burkina Faso during August 2006:

- Observations and resulting parameterisations for MCS anvil ice particle size distributions as function of potential temperature,
- Case studies of the microphysical properties in young and aged West African MCS outflows at the bottom of the TTL,
- Evidence for homogeneous new particle formation inside the anvil outflows,
- New data for upper tropospheric West African SVC cloud particle size distributions and a resulting parameterisation,
- Measurements of the fraction of ice cloud particle concentrations to interstitial aerosol particle number densities inside SVC, MCS anvils, and outflows.

2 Atmospheric context of the SCOUT-AMMA field campaign

The SCOUT-AMMA field campaign was based in Ouagadougou, Burkina Faso (at 12.2° N, 1.50° W), and took place from 31 July until 16 August 2006, at the beginning of a westerly Quasi-Biennial Oscillation (QBO) phase and within the West African monsoon wet season (Cairo et al., 2010b). Here, we briefly describe the atmospheric

ACPD
11, 745–812, 2011

situation from a trace gas measurement perspective. Homan et al. (2010) used CO, CO_2, and other trace substances to show that convection transported air from the boundary layer into the TTL which significantly influenced the trace gas composition of the air between 350 K and 370 K potential temperature, i.e. the outflow region. Based on domain filling trajectory ensembles from West Africa Law et al. (2010) showed that most air masses were already residing in the TLL during the 10 days prior to the measurements. Up to 39% of the air masses in the mid-TTL below 370 K were influenced by lower tropospheric air originating from Asia and India. Fierli et al. (2010) demonstrated for the 2006 monsoon season that detrainment effects from deep convection of MCSs are seen at 17 km altitude and possibly higher. Residues from biomass burning were detected on the M-55 “Geophysica” flight from 13 August 2006 in the TTL. These were traced back to biomass burning events in Central Africa (Real et al., 2010). Khaykin et al. (2009) provide evidence for overshooting convection over West Africa and for hydration within the TTL and lower tropical stratosphere due to evaporation of ice crystals. Finally, isentropic mixing of extratropical stratospheric air and transport across the subtropical tropopause can play a role for the composition of the air in the upper troposphere and TTL (Homan et al., 2010).

3 Instrumentation for cloud particle, submicron aerosol particle and trace gas measurements

3.1 Cloud particle size distributions and ice water content

A combination of measurements by a modified Particle Measuring Systems (PMS) Forward Scattering Spectrometer Probe (FSSP-100) with Droplet Measurement Technologies (DMT) high speed electronics (SPP-100) and a DMT Cloud Imaging Probe (CIP) was used to derive cloud particle size distributions. These probes cover a size range of 2.7 µm $< D_p <$ 31 µm (FSSP-100) and 25 µm $< D_p <$ 1600 µm with a 25 µm resolution (CIP). The characteristics of the instruments are described in detail in De Reus et al.

ACPD
11, 745–812, 2011

(2009, and references therein). While the time resolution of FSSP-100 measurements was set to 2 s, the CIP detects single cloud particles with a maximum sample rate of 8 MHz. Nevertheless, in order to combine with the FSSP-100 data also two second averages have been calculated for the CIP data. The uncertainties of the number concentration measurements of both probes are mainly determined by the uncertainties in the sample volumes, which were estimated to be 20% (Baumgardner et al., 1992). Additional uncertainty due to counting statistics has to be taken into account especially in conditions with low particle number concentrations.

In order to derive particle sizes from the CIP images a set of corrections needs to be applied. The underlying types of corrections are summarised in Table 1 (as in De Reus et al., 2009, if not specified otherwise) together with a short description and the corresponding references. The particle diameters derived from CIP measurements are specified in this paper by using the maximum dimension (Heymsfield et al., 2002). The Ice Water Content (IWC) was calculated using the scheme of Baker and Lawson (2006) in order to take into account the shape of the ice particles. The effective radius (r_{eff}), as a measure for the cloud radiative properties, is defined here as the ratio of the third to the second moment of a size distribution, in terms of spheres of equivalent cross-section area (McFarquhar and Heymsfield, 1998).

3.1.1 Shattering of ice particles on the cloud particle probes

A widely discussed problem for in-situ ice particle measurements is the shattering of ice crystals on the probe's arm tips and shrouds or inlets (e.g., Field et al., 2006; Lawson et al., 2008; Jensen et al., 2009). Since clouds in MCS outflows are likely to contain large particles and possibly high number concentrations artefacts introduced by shattering have to be considered. In contrast, the subvisual tropopause cirrus do not contain large particles (i.e. most particles are smaller than ≈100 µm) such that shattering can be considered to have only minor impact or even can be neglected (Lawson et al., 2008; Jensen et al., 2009). Furthermore, these clouds only have low number concentrations of particles. Also measurements in young contrails have been found to not be affected by shattering (Voigt et al., 2010).

ACPD
11, 745–812, 2011

For the cirrus clouds encountered by the M-55 "Geophysica" during the tropical campaigns TROCCINOX (Brazil, 2005; Huntrieser et al., 2007), SCOUT-O3 (Australia, 2005; Brunner et al., 2009; Vaughan et al., 2008), and SCOUT-AMMA intercomparisons were performed between the directly measured volume backscatter ratio (from the MAS instrument, see section below) and the corresponding values calculated from the FSSP-100 size distributions by Cairo et al. (2010a). According to their study the fraction of the size distribution detected by the FSSP-100 (i.e., 2.7 µm to 31 µm) well reproduces the cirrus optical properties in the visible part of the spectrum extending over backscattering cross sections of five orders of magnitude. If the FSSP-100 measurements had suffered from significant artificial enhancements by shattered ice particle fragments, the backscatter cross sections derived from FSSP-100 size distributions would differ from the MAS results because in this size range the backscatter ratio sensitively depends on the size distribution. For this reason we believe that shattering does not play a major role under the circumstances encountered in the cirrus clouds analysed by Cairo et al. (2010a).

However, to further cope with shattering artefacts the interarrival time technique, as proposed by Field et al. (2006), has been applied to the CIP data set. Therefore, the interarrival time threshold, below which particles are rejected, has been chosen individually for each flight according to the measurement characteristics and ranged between 2.6×10^{-6} s and 5×10^{-6} s. Unfortunately, the interarrival time method is not applicable for FSSP-100 measurements. However, with this technique time periods can be identified from the CIP data where measurements are affected by shattering. In case that there is very little or no shattering obvious in the CIP data, shattering is assumed to be within the instrument uncertainty for FSSP-100 data. In these cases the size distributions of both instruments show a good agreement for the size range (25 µm to 31 µm) where both instruments overlap. When looking at the frequency of occurrence of shattering, in 41% of the two second measurement time steps (i.e. data points) where clouds occurred no shattering has been measured by the CIP. For 85% of the data points with cloud occurrence the fraction of shattered particles is less than

ACPD
11, 745–812, 2011

20%. This lies within the instrumental uncertainty of the CIP. It has to be noted that the highest contribution to shattering was measured on the flight of 16 August 2006, where only 8% of the cloud data were not affected by shattering. Data are eliminated from further analyses in case that there is a high fraction of shattering in the CIP measurements. Size distributions also are excluded from further analyses in cases where the CIP and FSSP-100 size distributions do not make up a good match in the overlapping size range. This is so far the best possible approach until studies become available which quantify the shattering of the FSSP-100 as function of cloud particle size and number densities in cirrus clouds, as well as aircraft speed and ambient pressure. For this reason the results from the FSSP-100 measurements presented here constitute an upper limit estimate on the size distributions while the CIP data are fully corrected for shattering effects according to the current status of technology. De Reus et al. (2009) compared IWCs derived from in-situ hygrometer (FISH and FLASH) and particle (CIP and FSSP-100) measurements obtained during SCOUT-O3. Within the (large) measurement uncertainties the closure of these two very different measurement techniques was remarkable for the range of encountered IWCs between $10^{-5}\,\mathrm{g\,m^{-3}}$ and $10^{-2}\,\mathrm{g\,m^{-3}}$. If shattering had significantly altered the FSSP-100 results, discrepancies between the IWCs derived from the hygrometer and the particle measurements could have been expected for part of the covered IWC range. Since the IWCs encountered during SCOUT-AMMA in West Africa were of the same magnitudes as in SCOUT-O3, we believe that shattering did not significantly alter IWCs and hope the same holds for the FSSP-100 size distributions under these circumstances.

3.2 Submicron aerosol particle number densities, and optical properties

Ambient aerosol number concentrations were measured for particles with size diameters between lower detection limits of 6 nm (N_6), 10 nm (N_{10}), 15 nm (N_{15}) and roughly 1 µm as upper limit by three channels of the COndensation PArticle counting System (COPAS; Curtius et al., 2005; Weigel et al., 2009; Borrmann et al., 2010). In a fourth channel the sampled aerosol was heated to 250 °C such that only particles containing

ACPD
11, 745–812, 2011

non-volatile residues (with sizes above 10 nm) were detected and counted. The total accuracy is ±10% and COPAS samples with a frequency of 1 Hz. New particle formation (NPF) or nucleation events were encountered during some of the flights. These are associated with particle number densities N_6 being much larger than N_{15} or N_{10} as well (Weigel et al., 2011). Part of the M-55 "Geophysica" instrumentation was a Multi-wavelength Aerosol Scatterometer (MAS; for details see Cairo et al., 2004; Buontempo et al., 2006; Cairo et al., 2010b), which is a backscatter sonde for in-situ measurements of optical air, aerosol, and cloud parameters like volume backscatter ratio and depolarisation ratio (at 532 nm and 1064 nm). MAS samples with a time resolution of 5 s and has a precision of 10%.

3.3 Gas-phase species: NO_y, NO, CO, CO_2, O_3, and H_2O

Air originating from the cloud interior can be identified within MCS outflows by using trace gas data of CO, CO_2, NO_y, and NO.

Nitrogen oxide, NO, and reactive nitrogen species, NO_y were measured aboard the M-55 "Geophysica" with the StratospherIc Observation Unit for nitrogen oXides (SIOUX) two channel NO_y instrument (Voigt et al., 2005, 2007, 2008). During SCOUT-AMMA on most flights NO and gas phase NO_y were measured with two backward facing inlets of the SIOUX instrument using the chemiluminescence technique. In the NO_y channel gas phase NO_y is catalytically reduced to NO with CO in a gold converter heated to 300 °C. Thereafter the chemiluminescence reaction of NO with O_3 in the infrared is detected with two photomultipliers. The instrumental error is 10%, and the detection limit for NO and NO_y is better than 1 pmol/mol and 5 pmol/mol for a sampling frequency of 1 Hz.

CO_2 mixing ratios were measured in-situ on the M-55 "Geophysica" by a non-dispersive infrared absorption sensor (LI-COR 6251) that is part of the High Altitude Gas Analyzer (HAGAR), which also comprises a 2-channel gas chromatograph (Volk et al., 2000; Homan et al., 2010). For the CO_2 measurements during SCOUT-AMMA the time resolution was 5 s and the flight-to-flight precision about 0.3 µmol/mol.

ACPD
11, 745–812, 2011

Mainly for the identification of biomass burning events in-situ carbon monoxide measurements were performed by the Cryogenically Operated Laser Diode (COLD; Viciani et al., 2008) instrument, which has at a lower detection limit of a few nmol/mol, an accuracy of 6–9% and a precision of 1%.

Ozone mixing ratios were obtained at 1 Hz sampling rate from the Fast OZone ANalyzer (FOZAN; Yushkov et al., 1999; Ulanovsky et al., 2001) with an accuracy of 10%.

Total water was measured as sum of water condensed in ice particles and gas phase water with a forward facing inlet by means of a Fast In-situ Stratospheric Hygrometer (FISH). Its Lyman-α photofragment fluorescence technique is described in Zöger et al. (1999). Due to the inlet geometry the ice particles are sampled with an enhancement, thus, the contribution of ice to the total water has to be corrected afterwards. The methods underlying the ice particle detection are described in Schiller et al. (2008). The rearward/downward facing FLuorescent Airborne Stratospheric Hygrometer (FLASH) (Khaykin et al., 2009; Sitnikov et al., 2007) was used to measure only the gas phase water such that the ice water content could be determined in conjunction with the FISH total water. In combination with concurrent temperature measurements also the saturation with respect to ice could be calculated. The uncertainties of the FISH data are 6% or 0.2 µmol/mol and the corresponding values for FLASH are 8% and 0.3 µmol/mol (Krämer et al., 2009).

The ambient temperature was measured using a Thermo Dynamic Complex (TDC) with an accuracy of 0.5 K (Shur et al., 2007), while other relevant parameters as position and true air speed have been adopted from the aboard navigational system UCSE (Unit for Connection with the Scientific Equipment; Sokolov and Lepuchov, 1998).

In West Africa the ambient and operational conditions on the ground and during the flights were extremely challenging for all instruments. For this reason the measured parameters are not always available for each flight or the entire flight.

ACPD
11, 745–812, 2011

4 Results and analyses

The data base from the SCOUT-AMMA campaign includes data of a total of nine flights. The FSSP-100 and CIP were operated simultaneously during five flights: 7, 8, 11, 13, and 16 August 2006 (transfer flight). During one flight (13 August 2006) only low level clouds have been probed.

4.1 Overview of the MCS anvil measurements

During the SCOUT-AMMA flights of the M-55 "Geophysica" anvils of MCS were penetrated at altitudes between 345 K and 365 K of potential temperature altitude. The ice particle size distributions from these encounters are shown in Fig. 1 including some distributions from SVC in the second and third panels. The measurements were performed with averaging times of 10–20 s resulting in good counting statistics for the majority of the cases. In the other cases, as for example encounters of SVC (see Sect. 4.5) with low number concentrations the averaging time needed to be individually adapted and ranges up to 200 s. All size distributions are classified in 10–20 K bins of potential temperature ($T_{\mathrm{potential}}$) and are normalised to a total $dN/d\log D_{\mathrm{p}}$ value of 1 (as in De Reus et al., 2009). The thin black lines represent the individual measurements while the red lines denote the median size distribution of each potential temperature bin. It can be seen that the maximum particle sizes are decreasing when ascending into the tropopause region ($365\,\mathrm{K} < T_{\mathrm{potential}} < 385\,\mathrm{K}$). This agrees with the measurements obtained during the SCOUT-O3 campaign in Northern Australia (De Reus et al., 2009), of which the medians are shown in blue. In that study also stratospheric clouds, originating from Cb overshoots, had been probed and are displayed here as thin blue lines in the uppermost panel ($T_{\mathrm{potential}} > 385\,\mathrm{K}$) for comparison. A parameterisation for tropical cirrus had been derived from ice crystal size distribution measurements during the Central Equatorial Pacific Experiment (CEPEX) by McFarquhar and Heymsfield (1997). Tropical anvil cirrus had been probed there with ice water contents ranging from 10^{-4} to $1\,\mathrm{g\,m^{-3}}$ and at ambient temperatures between 253 K and 203 K. Adopting the CEPEX parameterisation, curves of the normalised particle size distributions were calculated for the West African and Australian measurements. For this the average IWCs and ambient temperatures as observed are taken as input for the calculations. We have to note that the temperatures observed during the SCOUT-AMMA campaign were lower (i.e., ranging between 195 K and 210 K) than during CEPEX. The results of the calculations are shown in the broad pale red lines for SCOUT-AMMA and in the broad pale blue lines for SCOUT-O3. The size distributions resulting from the parameterisations have a similar decrease in maximum particle size with increasing potential temperature in the troposphere. However, they show a more pronounced mode at diameters of 100–200 µm, which is not present in our observations. Furthermore, the CEPEX parameterisation clearly underestimates the concentrations for large particle sizes in the lowest potential temperature bin. In the 355–365 K bin measurements are fewer but still particle sizes are larger than those calculated from the parameterisation. Particularly in the CIP size range, the shape of the size distributions indicates a higher fraction of large particles than deduced by the CEPEX parameterisation. Since the CEPEX parameterisation is a result of measurements from the Maritime Continent while SCOUT-AMMA took place over West Africa, the discrepancy possibly confirms the observation by Cetrone and Houze (2009) according to which the continental MCS tend to produce larger hydrometeors. Why the CEPEX parameterisation fails to reproduce the (maritime) measurements of SCOUT-O3 over the Tiwi-Islands near Darwin (Australia) remains unanswered, though.

In order to describe the ice particle size distributions from SCOUT-AMMA for each potential temperature bin (as in Fig. 1) two or three modal lognormal distributions are fitted to the now not normalised median size distribution $n_*(D_\mathrm{p})$, following

$$n_*(D_\mathrm{p}) = \frac{dN}{d\log D_\mathrm{p}} = \sum_i \left(\frac{N_i}{\sqrt{2\pi}\log\sigma_i} \exp\left[-\frac{(\log D_\mathrm{p} - \log\overline{D_{\mathrm{p}i}})^2}{2(\log\sigma_i)^2} \right] \right). \quad (1)$$

Here, D_p is the particle diameter in µm, i the number of modes (two or three), N the

Discussion Paper | Discussion Paper | Discussion Paper | Discussion Paper |
ACPD
11, 745–812, 2011
Tropical ice clouds: MCS outflow, anvil, and subvisual cirrus
W. Frey et al.

number concentration (cm^{-3}), $\overline{D_p}$ the mean modal diameter (µm), and σ the standard deviation. The $n_*(D_p)=dN/d\log D_p$ values result in cm^{-3}. The parameters of the fitted functions are comprehended in Table 2, similar to Table 1 in De Reus et al. (2009) for the SCOUT-O3 measurements in Northern Australia.

4.2 Case study 1: young MCS outflow in the West African upper troposphere

4.2.1 Atmospheric context and gas phase species

During the descent of the flight on 7 August 2006 the M-55 "Geophysica" crossed a layer of air which can be characterised as young or recent outflow from an MCS. Trajectory analysis (Fierli et al., 2010) indicate an age of less than three hours. The EUMETSAT/ESA Meteosat Second Generation satellite image of the MCS constellation at the time of the measurements is shown in Fig. 2 together with the M-55 "Geophysica" flight track, in blue for the concurrent part of the satellite image, in red for the whole flight. In Fig. 3 the vertical profile measurements are displayed for: temperature (T), relative humidity with respect to ice (RHi), O_3, NO, NO_y, cloud particle concentrations (N_{cloud}), and ice water content (IWC), as well as the N_{15} and ultrafine particle concentrations (denoted as $N_{6-15}=N_6-N_{15}$ in the figures). The thermal tropopause was located at 370 K and well defined. The presence of slightly elevated cloud particle number densities and IWC in the fourth panel of Fig. 3 between 365 K and 370 K show an SVC which was located directly beneath the tropopause. This cirrus Case SVC2 is further discussed in Sect. 4.5. Below 355 K a layer of air was located which had relative humidities between 60% and 140%, and contained an ice cloud with IWCs around 5×10^{-3} g m^{-3} and with ice particle number densities of roughly 5 cm^{-3}. Slightly enhanced CO mixing ratios have been observed in this cloud band. In the lower part of the cloud (below 350 K) elevated NO and NO_y mixing ratios were detected, even reaching values above 10 nmol/mol. These constitute very high values, indicating that the cloud layer is a young outflow from the small (≈60 km in diameter) MCS at the Eastern

ACPD
11, 745–812, 2011

part of the blue flight track line in Fig. 2, which is just developing. (Note: The general flow direction as seen from subsequent satellite images and trajectory analyses is from East to West in this location and altitude band.)

4.2.2 Aerosol and cloud measurements

A zoom-in on the flight data time series during the cloud layer crossing is shown in Fig. 4 and selected cloud particle size distributions of the time periods which are shaded in blue are compiled in Fig. 5. These are labelled as above-outflow Cases "AOF1" and "AOF2", and outflow Cases "OF1" and "OF2". Apparently, the cloud layer vertically extended from 13.2 km to 11.0 km altitude and within this cloud band three sub-layers can be discerned. The uppermost sub-layer (denoted as "Sub-layer 1" in Fig. 4) contained lower cloud particle concentrations in coincidence with a strong in-cloud New Particle Formation event (NPF). The details of this NPF are analysed in Weigel et al. (2011) and juxtaposed with other NPFs in the tropical UT/LS from different locations. Based on the ice particle data this cloud segment can be considered as MCS anvil part but the low values for NO and NO_y indicate that this is *not* an outflow from the MCS. The second cloud sub-layer (denoted as "Sub-layer 2") also was a part of the MCS anvil where the cloud particle number density increased by almost a factor of 10 and where the nucleation event was "quenched". Below, from 56 385–56 557 s UTC, the third cloud sub-layer ("Sub-layer 3" in Fig. 4) extended between 11.9 km and 11.0 km involving high particle number concentrations and very high values for NO and NO_y. This is the MCS outflow where the detrainment must have occurred very recently, since the elevated NO and NO_y had not been diluted yet. Also very little of the NO had been oxidised to NO_y by the time of the measurement. From the enlarged satellite image and the flight track of the aircraft one can estimate that the sampling occurred at a maximum distance of roughly 30 km from the source region of the NO_x. The cloud particle size distributions show that the clouds at the highest cloud level in "Sub-layer 1" contained no particles larger than 400 µm. As the aircraft descended, the concentrations and particle sizes increased to 8 cm^{-3} and

1.6 mm, respectively. During "AOF2" and in particular during "OF1" it can be assumed that there also were particles with sizes much above the CIP detection limit. Examples of some individual cloud particle shadow cast images obtained from the CIP are shown in Fig. 6. As far as one can tell from visual inspection these mostly seem to be heavily rimed ice particles or rimed aggregates.

4.3 Case study 2: aged MCS outflow at 14 km altitude

4.3.1 Atmospheric context

During the flight of 11 August 2006 the M-55 "Geophysica" flew through a region behind a squall line with horizontal extension of approximately 1000 km (see the cloud band roughly aligned with the -3° W meridian in the satellite image of Fig. 7). The structure of this particular MCS is described in Chong (2010) using data by the MIT Doppler radar. The aircraft crossed the outflow region between 300 km and 400 km behind the squall line, which is much further away from the MCS core region than in Case study 1. Although NO and NO_y measurements are not available from this flight, it can be assumed that a more aged MCS outflow air mass was probed than on 7 August 2006. Trajectory analysis indicate an age of these outflow clouds of about 10 h. Here, we use CO_2 data to identify outflow regions.

4.3.2 Overview of vertical profiles

The vertical profiles of the measured variables are presented in Fig. 8. They include measurements from ascent, descent, and one dive. Thus, spreads in the single parameters might result from the profiling at different locations. The thermal tropopause was located near 16.5 km (i.e., 375 K). The relative humidity is presented as ten second running average since the FLASH measurements were noisy during this flight. Therefore, the relative humidity as calculated from the FISH total water content ($RHi_{enhanced}$, not corrected for enhanced ice particle sampling, see Sect. 3.3) is displayed additionally.

ACPD
11, 745–812, 2011

Cloudy parts show thus a clear enhancement from the gas phase baseline in the relative humidity. The relative humidities from the FLASH and the FISH baselines show good agreement. In the second panel the vertical profile of CO_2 exhibits a distinctive minimum between 353 K and 360 K, which indicates the presence of air from lower altitudes. Most likely this air mass was convectively uplifted from the boundary layer, where the vegetation metabolises CO_2. The third panel in Fig. 8 shows that patchy clouds existed at all altitudes above 351 K up to the tropopause with low ice particle number concentrations ($\approx 10^{-2}\,cm^{-3}$). In particular, tenuous clouds were present in the altitude band with the low CO_2 mixing ratios. At the same time the remnants of an NPF event are discernible in the fourth panel which partly occurred inside the outflow cloud and partly outside the cloud but still within the outflow. The ultrafine particle concentrations (N_{6-15}) attained values as high as $1000\,cm^{-3}$. Interestingly, the non volatile fraction (see panel 5) of these newly formed aerosol particles is very low (5%) inside the outflow while it is much higher (50%–60%) above. This indicates that the newly formed particles consist mostly of sulfuric acid and water as shown by Weigel et al. (2009) and Curtius et al. (2005).

4.3.3 New particle formation event

A closer look on a flight segment from 58 200 s UTC to 58 400 s UTC is presented in Fig. 9. The blue shaded area designates the crossing of a cloud patch as indicated by the cloud particle number densities (in brown). The occurrence of an NPF between 58 200 s UTC and 58 350 s UTC can be inferred from the four coloured, dotted lines of COPAS data for $N_{aerosol}$. (1.) The absolute number of particles with sizes above 6 nm (as depicted with the grey dotted line) is unusually high. (2.) The number density difference N_{6-15} (yellow dotted line) exceeds 900 particles per cm^3 during this flight segment. This is the case inside the cloud patch but also, and more pronounced, in the peak outside of the cloud around 58 325 s UTC. (3.) The other coloured dotted lines of additional COPAS data show mostly non-zero differences also for N_{6-10} and N_{10-15} (green and red dotted lines). The low mixing ratios concurrently measured for CO_2

Discussion Paper | Discussion Paper | Discussion Paper | Discussion Paper |
ACPD
11, 745–812, 2011
Tropical ice clouds: MCS outflow, anvil, and subvisual cirrus
W. Frey et al.
Title Page
Abstract Introduction
Conclusions References
Tables Figures
◀| |▶
◀ ▶
Back Close
Full Screen / Esc
Printer-friendly Version
Interactive Discussion

indicate that both, NPF and cloud event occurred inside an MCS outflow. If the values for $N_{10–15}$ are small, only few newly formed 6 nm particles have grown by condensation or coagulation to sizes above 10 nm and still below 15 nm. Or some of the newly formed 6 nm particles have already been lost to the surfaces of the preexisting background particles. This seems not to be the case during the cloud crossing because N_6 as well as $N_{10–15}$ remain constant at ≈1000 cm^{-3} and ≈400 cm^{-3}, respectively. Before the cloud encounter and especially at the strong peak after (around 58 325 s UTC) $N_{10–15}$ is larger, which indicates that a higher fraction of the freshly nucleated particles has grown in size beyond 10 nm. For the whole flight segment shown in Fig. 9 we inspected the COPAS internal housekeeping data (e.g., flow rates, stability of temperature settings etc.) with particular care in order to identify possible instrumental artefacts. However, COPAS operated well during this flight segment and we conclude that the M-55 "Geophysica" had indeed encountered an NPF event.

4.3.4 Entrainment and isobaric mixing as possible mechanism for the NPF peak

From the abscissa for the covered flight distance in Fig. 9 it can be seen that the horizontal scale of the NPF peak between 58 310 s UTC and 58 350 s UTC was quite small (roughly 6 km). Also its vertical extent is only 300 m. During these forty seconds flight time the CO_2 had increased towards the typical UT/LS background levels. The data summarised in Table 3 provide evidence that two adjacent layers of very different properties were stacked upon each other here. The times of the begin and end of the NPF peak were chosen for comparison of the different parameters. The upper layer was dry (with RHi<38%) and accomodated a non-volatile fine particle fraction of 50%, while the lower layer contained more water vapour (RHi of 80%) and only 6% (or less) of the fine aerosol particles were non-volatile. Since the lower layer constituted the aged MCS outflow air the values listed in the table indicate that entrainment and mixing might have been proceeding concurrently creating a supersaturated environment for binary sulphuric acid-water solution droplets and initiating the peak in the NPF. The possibility of such processes was pointed out by Khosrawi and Konopka (2003).

ACPD
11, 745–812, 2011

4.3.5 Cloud particle observations within the aged MCS outflow

The particle size distribution of the cloud crossing is shown in Fig. 10 in the lower left panel. Obviously, the cloud particles were much smaller and fewer than those in the young outflow of Case Study 1 (see Fig. 5). As the relative humidities during this event were below 100% the cloud patch of this outflow was dissipating. The other cloud particle size distributions given in Fig. 10 in the upper panels are from similar cloud crossings of the same MCS in different outflow locations which were somewhat closer to the squall line. In addition the lower right panel displays further measurements of size distributions (blue lines) from above and below the outflow. Again, in general only small ice particles were detected in very low number concentrations. However, the cloud particles outside of the outflow zones were somewhat larger than inside.

4.4 Case study 3: cross section through MCS anvil of 7 km thickness

On the ascent on 16 August 2006 the anvil of an MCS of roughly 400 km in diameter has been probed (see Fig. 11). The clouds have been observed up to an altitude of 15.1 km which corresponds to 363 K potential temperature. The distance to the core region of the MCS was estimated from the satellite image to about 300 km. No tracer measurements are available for the lowest 7.8 km of the cloud. However, the level of main MCS outflow is expected at higher altitudes. Here, measurements of of CO_2, NO, and NO_y are available and are presented in the vertical profiles of Fig. 12. Based on the temperature and ozone measurements the cold point tropopause was found at 15.4 km altitude and 366 K potential temperature. Since FLASH data were not available for this flight, the FISH total water content was used to calculate $RHi_{enhanced}$, as for the flight on 11 August. Cloudy parts show thus a clear enhancement from the gas phase baseline in the relative humidity. In the altitude band between 348 K and 362 K NO and NO_y mixing ratios are elevated as well as CO_2 mixing ratios are reduced which provides evidence for having encountered a convective outflow region. This is supported by trajectories which indicate an outflow age of around five hours. Remarkably, the O_3 shows

Discussion Paper | Discussion Paper | Discussion Paper | Discussion Paper |

ACPD
11, 745–812, 2011

Tropical ice clouds: MCS outflow, anvil, and subvisual cirrus

W. Frey et al.

a small maximum in the altitude band between 342 K and 348 K. Since no correlation to NO or NO_y can be found here, these enhanced ozone mixing ratios did not result from the recent outflow event and concurrent photochemical production but could be due to downwind production of O_3 from lightning NO_x emissions produced by an MCS upwind or due to uplift of soil NO_x emissions which are more elevated over the Northern Sahel region (Barret et al., 2010). A closer look on the cloud crossing in the time series of the ascent in Fig. 13 reveals that the cloud can be divided into three parts. The first part reaches from the ground to 4.8 km altitude. Here, only particles smaller than 20 µm were observed by the FSSP-100 while the CIP showed no counts (see the size distribution in the upper left in Fig. 14). These could be remnants of evaporating precipitation, haze droplets or large aerosol particles. The latter could either be resuspended from the ground by the gust fronts or grown to size by water uptake. Also the Colour Index (CI), defined from the MAS backscattering measurements at 1064 nm and 532 nm (as in Liu and Mishchenko, 2001), gives high values in this layer, indicating scattering predominantly from larger aerosol particles. The second cloud layer extended from 5.7 km to 10.6 km (between the two local minima of the cloud particle number concentration in Fig. 13). The abrupt change in CI indicates the presence of a different type of cloud particles which are much larger as indicated by the low CI values. At the lower part of this layer the CIP imaged very large ice cloud particles as snow flakes and aggregates. A few examples are shown in Fig. 15. Tracer measurements are not available during the first part of the layer crossing. Towards the end of the encounter CO_2 mixing ratios were rather high and NO mixing ratios low which implies that there was no outflow. The third cloud layer between 10.6 km to 15.1 km altitude contained outflow signatures in the tracer data. As evident from the size distribution in the lower left of Fig. 14 again only small particles were detected by the FSSP-100 at the end of this layer. Further size distributions of selected time periods, as shaded in blue in Fig. 13, are displayed in Fig. 14. Two of the size distributions were measured below the outflow in the second cloud part ("BOF1" and "BOF2") and three inside the outflow ("OF3" to "OF5") region. In general, the outflow size distributions show similar values for the number densities,

ACPD
11, 745–812, 2011

only the maximum particle sizes decrease slightly with altitude. In comparison to the young outflow event on 7 August the size distributions from 16 August show similar but somewhat lower concentrations and sizes. However, a clear difference to the aged outflow events of 11 August is obvious. Considering the satellite picture and the distance to the MCS core region, the event of 16 August was a recent outflow. The difference between the NO and NO_y mixing ratios is larger than for the young outflow of 7 August which indicates that parts of the NO had already been oxidised. A conclusion could be that the outflow air of 16 August had undergone longer chemical processing than on 7 August.

4.5 In-situ measurements of subvisual cirrus over West Africa

Only few in-situ measurements of cloud particle size distributions inside subvisual cirrus (SVC) are reported in the literature. Those measurements originate from the tropical West Pacific in 1973 (Heymsfield, 1986; McFarquhar et al., 2000); the Indian Ocean during APE-THESEO in 1999 (Luo et al., 2003a,b; Peter et al., 2003; Thomas et al., 2002); the Meso American Pacific during CRAVE, 2006, (Lawson et al., 2008); and from the equatorial Eastern Pacific during TC4 in 2007 (Davis et al., 2010). The measurements presented here are the first data obtained over West Africa. These extend the known data set of tropical SVC and also contribute *continental* measurements while the other observations were from *maritime* regions. During the research flights of SCOUT-AMMA four subvisual cirrus clouds were encountered close to the tropopause and within the TTL over West Africa. The detailed size distributions compiled from these events (denoted as SVC1 to SVC4) are displayed in Fig. 16 with the measured microphysical parameters summarised in Table 4. None of the observed ice particles is larger than 130 µm in diameter and during none of these events the CIP detected any shattering. Therefore, it is unlikely that the FSSP-100 measurements inside these SVC are noticeable affected by shattering. The CIP measurements can not distinguish particle shapes because too few pixels are shaded in the 25 µm-resolution. However, Lawson et al. (2008) analysed the shapes of the tropical SVC particles and found that

ACPD
11, 745–812, 2011

they are quasi-spherical and hexagonal. Under these circumstances (i.e., the absence of highly aspherical small ice crystals) particles smaller than roughly 16 µm can be reliably sized by the FSSP-100 (Borrmann et al., 2000). For the particles above 25 µm the CIP image analyses were applied as described above. Thus, between 16 µm and 25 µm some uncertainty remains with respect to the sizing of the potentially aspherical particles by scattered light measurements of the FSSP-100. This may be the reason for the "spike" occasionally found in the fourth size bin in Fig. 16.

The duration of the cloud encounters (i.e. averaging time for the size distributions) ranged between 52 s and 143 s, the clouds were observed in altitudes between 15 km and 16.4 km, and at potential temperatures between 363 K and 373 K. The local cold point tropopause on these days was located at about 16.3 km altitude on 7 August 2006 and at about 16.5 km altitude on 8 and 11 August 2006. Thus, three of the subvisual clouds were observed a few hundred meters below the tropopause while one case (SVC2 on 7 August 2006) was encountered directly at tropopause altitude. The lowest temperature inside the SVCs was observed during the encounter of SVC1 (192 K) which also had the lowest number concentration and IWC. The warmest cloud was SVC3 with temperatures of 198 K and here, the highest number concentrations and largest IWC were detected. Although the difference between these temperatures is not large, the corresponding saturation vapour pressures with respect to ice differ by a factor of 2.7 which influences the capability of the clouds for freeze-drying the air ascending through them. (For comparison, the temperatures observed for the SVC by Lawson et al. (2008) were between 183 K and 198 K, by Davis et al. (2010) between 193 K and 198 K, and by Thomas et al. (2002) between 192 K and 197 K.)

In order to relate the West African measurements to the overall picture of available SVC size distribution data, a summarising graph is presented here in the left panel of Fig. 17 which extends the original figure shown in Davis et al. (2010). The events observed during SCOUT-AMMA, represented by the thin coloured lines, generally fit well into the previous data from other regions (thick grey lines) and all size distributions show that there are no particles larger than 200 µm inside SVCs.

ACPD
11, 745–812, 2011

In the West African SVCs the measured ice crystal number concentrations range between $2\times10^{-3}\,\mathrm{cm^{-3}}$ and $2.4\times10^{-2}\,\mathrm{cm^{-3}}$, the IWCs range from $3\times10^{-6}\,\mathrm{g\,m^{-3}}$ to $3.8\times10^{-4}\,\mathrm{g\,m^{-3}}$, and the effective radii from 2.3 µm to 20.9 µm. These values are comparable to those obtained from the measurements in the maritime area of Costa Rica during the CRAVE campaign. For example the effective radii reported there lie between 2.44 µm and 16.7 µm and the IWCs vary from $1.2\times10^{-5}\,\mathrm{g\,m^{-3}}$ to $50\times10^{-5}\,\mathrm{g\,m^{-3}}$. The largest sizes found over maritime Middle America were 165 µm. However, in comparison to the measurements obtained over the West Pacific and during CRAVE the West African observations exhibit concentrations which are more than an order of magnitude lower for particles below 10 µm. At the same time, the events SVC2 and SVC3 show higher concentrations for particles with sizes larger than 50 µm with respect to CRAVE and TC4. Possibly due to the contribution of these large particles the two West African events at the same time have higher IWCs (i.e., of $1.5\times10^{-4}\,\mathrm{g\,m^{-3}}$ to $3.8\times10^{-4}\,\mathrm{g\,m^{-3}}$ compared to $5.5\times10^{-5}\,\mathrm{g\,m^{-3}}$ in CRAVE and $5.6\times10^{-6}\,\mathrm{g\,m^{-3}}$ in TC4).

Despite such differences in details the size distributions $n_*(D_\mathrm{p})$ for tropical SVC from the literature are similar enough to calculate a parameterisation. The result of an exponential least squares fit according to

$$n^*(D_\mathrm{p}) = \frac{dN}{d\log D_\mathrm{p}} = A\cdot\exp\left(-\frac{D_\mathrm{p}}{\kappa\cdot D_{\mathrm{p}_0}}\right) \tag{2}$$

is shown in the right panel of Fig. 17. The $dN/d\log D_\mathrm{p}$ values result in $\mathrm{cm^{-3}}$, if D_p is supplied in µm. The coefficient A is $0.044422\pm0.0123\,\mathrm{cm^{-3}}$, $\kappa=13.98\pm6.08$, and $D_{\mathrm{p}_0}=1$ µm is used to eliminate the unit. As the one-sigma deviation lines in Fig. 17 demonstrate, this simple parameterisation seems to represent the tropical subvisual cirrus cloud size distributions quite well. Also the chi-square is calculated and results in $\chi^2=0.0367$. Thus, the fit might be useful for large and mesoscale modelling purposes, where the microphysical processes are not resolved and as long as not more data are available in order to formulate a parameterisation in terms of microphysical properties or processes.

Discussion Paper | Discussion Paper | Discussion Paper | Discussion Paper |

ACPD

11, 745–812, 2011

Tropical ice clouds: MCS outflow, anvil, and subvisual cirrus

W. Frey et al.

The size distributions from Fig. 16 exhibit a significant fraction of larger particles with sizes above 50 µm. This is of significance in the context of the stabilisation mechanism suggested by Luo et al. (2003b), who assumed smaller sized particles. Under the given thermodynamic conditions such large particles (50–200 µm) have terminal settling velocities ranging between roughly 10 mm s^{-1} and 1000 mm s^{-1}. Thus, as noted by Lawson et al. (2008), the prevailing vertical wind speeds are by far too small to lift these particles and therefore, extended SVCs containing such large particles can not be maintained by this mechanism.

Due to the lack of concurrent LIDAR observations for the measurements in West-Africa the horizontal extent of these SVCs is not known (unlike e.g. for the APE-THESEO case where the cloud sheet covered roughly 250 km). This implies that either the clouds were more localised with transient atmospheric conditions allowing for their existence, or the vertical wind velocities in the field of the propagating MCS were locally high enough to support larger ice particles. The subvisual clouds during SCOUT-AMMA were observed in a region influenced by strong convection and thus, might have formed as remnants of convective anvils. However, the tracer measurements obtained at the same time did not show any convective signatures. Either the time past the convection was long enough such that the air had mixed with surrounding air diminishing the convective signature, or the SVC had formed in-situ. Both mechanisms are recognised in the literature (e.g., McFarquhar et al., 2000; Pfister et al., 2001; Massie et al., 2002).

4.6 Interstitial aerosol number densities in SVC and MCS

In order to obtain an estimate of how many cloud particles result from activation of the present aerosol, it is instructive to plot the COPAS measurements as proxy for the available aerosol particle number densities versus the concurrently measured cloud particle number concentration. Since the number of cloud particles (partly also detected by COPAS) is much smaller than the submicron aerosol number densities, the contribution of the cloud particles to N_6, N_{10}, N_{15} can be considered as small or negligible. This

ACPD
11, 745–812, 2011

especially holds for the encountered upper tropospheric clouds because the ice particles are for the most part much larger than 1 µm which roughly is the upper particle size which the COPAS inlet is able to aspirate with proper efficiency. In Fig. 18 the results from the SVCs and the MCS outflows from West Africa (SCOUT-AMMA) are juxtaposed with data from the Hector MCS in Northern Australia (SCOUT-O3; see De Reus et al., 2009). Although the data base is small, the three different cloud environments can be clearly discerned. For the SVCs (which are described in Sect. 4.5) we found roughly one cloud ice particle per 30 000 detected aerosol particles. This is in agreement with the results from Jensen et al. (2010) who derived from model calculations that only very few aerosol particles can serve as ice nuclei for the activation of cloud particles in SVC. For the MCS outflow cases one cloud particle occurs per ≈1000 aerosol particles with some observations as high as one of 300. This difference between these numbers of the two cloud types may be indicative of the respective roles which deposition freezing and homogeneous freezing play for cloud formation. It also can be assumed that in the outflow cases all the mechanisms of ice multiplication (collisional multiplication, Hallet Mossop mechanism, splintering, and riming) play a major role. These are absent in SVC which formed ice particles (not larger than 200 µm) mostly by deposition nucleation. The values for the single MCS cluster Hector span the range between one over 30 000 and one over 300 with a clustering of points near the 1/3000 ratio line. As the light blue symbols indicate, NPF events could be identified for a few cases of the Hector MCS and also during SCOUT-AMMA. Since the figure only shows the concentration N_{15} the absolute numbers are relatively small. The values for N_6 as concurrently measured by COPAS were between 2000 and 3000 cm^{-3}. Here the difference between N_6 and N_{15} is large enough for identification as an NPF event. (For the two green squares and the four dark blue triangles with number densities N_{15} above 1000 cm^{-3} in Fig. 18 no N_6 data are available or the N_6–N_{15} difference was too small for an NPF event.) Based on the few measured points one could speculate that NPF events preferably occur under circumstances where only a few cloud ice particles are present.

ACPD
11, 745–812, 2011

These data are only an indirect estimate of the degree of cloud activation for these clouds. As pointed out by De Reus et al. (2009) the original activation ratio may differ from these measurements because there are sinks for particles such as scavenging by deposition on ice particles, washout by supercooled droplets, mixing with the local ambient air, and entrainment of cloud free air. As shown in Sect. 4.1 in-cloud NPF may be a source for ultrafine aerosol (Weigel et al., 2011). Although the very low ratios for the SVC cases indicate that deposition freezing might have formed these, a variety of processes which are not directly related to heterogeneous aerosol ice activation (e.g., homogeneous droplet freezing) may have been involved at varying intensities during the cloud lifetime in particular for the MCS outflows and Hector. For mid-latitude cirrus Seifert et al. (2004) found a positive correlation between the number concentrations of interstitial aerosols and ice crystals as long as the interstitial particle number densities were below 100 cm^{-3} and at higher aerosol concentrations a negative correlation was measured.

Despite such considerations the measurements in Fig. 18 provide data as boundaries for modelling purposes which may help to estimate the contributions of the different microphysical processes.

5 Summary and conclusions

In-situ observations of cloud ice particle properties have been obtained in the vicinity of MCS and within the tropical UT/LS at the time of the West African Monsoon during the SCOUT-AMMA campaign in Ouagadougou, Burkina Faso, in 2006. These data provide a contribution to the very sparse data set of in-situ measurements of MCS outflows and tropical SVC above an important continental area.

The observed ice crystal size distributions, were classified by means of potential temperature into altitude bins and compared to former measurements from the SCOUT-O3 campaign and the CEPEX parameterisation calculated for the SCOUT-

ACPD
11, 745–812, 2011

AMMA measurements. All show a decrease in maximum particle size when ascending to the tropopause region. However, the SCOUT-AMMA observations show clearly larger particles than observed during SCOUT-O3 and derived from CEPEX parameterisation as well as a higher fraction of large particles. Possibly this is due to the fact that these size distributions were obtained above a continental area in contrast to the former measurements above maritime regions. This would agree with the suggestion by Cetrone and Houze (2009) who deduce that due to the dry adiabatic temperature profiles above West Africa the convection there might be deeper and produces stronger precipitation with larger hydrometeors than compared to the Maritime Continent. Also Hall and Peyrille (2006) point out that due to the capping Saharan Air Layer (SAL) it is more usual that deep convection occurs in large scale energetic systems in West Africa. Two or three modal lognormal size distributions have been fitted to the West African measurements for each potential temperature bin in oder to provide a mathematical description of the continental MCS size distributions.

Trace gas observations and satellite images were used to identify MCS outflow events and to estimate the age of those events. For the latter, also trajectory analysis have been performed. Clouds within young outflow events were sampled on the flights of 7 and 16 August 2006, the former resulting from a newly developing system and the latter from a mature system. The particle images show heavily rimed ice particles or rimed aggregates with sizes even extending beyond 1.6 mm (i.e. the upper detection limit of the CIP). Ice crystal number concentrations of up to 8.3 cm^{-3} and IWCs of up to 0.05 $g\,m^{-3}$ were observed, the effective radius was about 90 µm. In contrast to this, clouds within the aged outflow events of the 11 August 2006 reveal much smaller values. Here, maximum concentrations of 0.03 cm^{-3}, IWCs of up to 2.3×10^{-4} $g\,m^{-3}$, and an effective radius of about 18 µm have been found with particles reaching a maximum dimension of 61 µm. The size distributions of all outflow events show a change with age which is displayed in Fig. 19. It can clearly be seen that the ice particles become smaller and fewer with increasing age. The snap-shots of consecutive CIP particle images, as shown on top of the figure, underpin the change in

ACPD
11, 745–812, 2011

size with age. Furthermore, the outflow altitude increases with age. This is supported by Houze (1989) who describes the upward transport of older convective cells within an MCS. These are advected rearward over a layer of dense, subsiding inflow.

Besides the measurements connected to MCS outflows four encounters of subvisual tropopause cirrus have occurred at altitudes between 15–16.4 km, which corresponds to a distance to the tropopause of 0–600 m. These observations extend the existing data set of tropical SVC and constitute the first continental SVC measurements. The largest particles had sizes of up to 130 µm, while the number concentrations ranged from $2 \times 10^{-3}\,cm^{-3}$ to $24 \times 10^{-3}\,cm^{-3}$, IWCs from $0.3 \times 10^{-5}\,g\,m^{-3}$ to $38 \times 10^{-5}\,g\,m^{-3}$, and the effective radii varied between 2.3 µm and 20.9 µm. The size distributions of the SVC events are compared to all so far known SVC size distributions and an exponential fit on all of these is calculated. We provide this parameterisation of SVC for modelling studies which is important since they play an important role in the Earth's radiation budget.

Differences in the aerosol depolarisation ratio and Colour Index observed by MAS between the measurements inside the MCS outflow clouds and the SVC were found: The aerosol depolarisation ratio showed medium to high values (40–100%) in the outflow events, and medium values (40–70%) in the SVC encounters. Similarly, the Color Index was small within the outflow, and slightly increased with altitude and in the SVCs. These observations suggest large depolarising particles in the MCS outflows. By contrast, the SVC seems to have more of smaller particles that possibly have a different morphology than those inside the outflows. The CIP shadow images obtained within the outflows show irregularly shaped ice crystals like aggregates, while for the SVC measurements the images were too small to distinguish a particular shape. However, shapes of SVC ice particles have been reported by Lawson et al. (2008) and Davis et al. (2010), both using a Cloud Particle Imager (CPI), who found primarily quasi-spherical particles and some plate-like hexagonal particels (Lawson et al., 2008). Columnar and trigonal particle shapes have been observed with a replicator (McFarquhar et al., 2000; Heymsfield, 1986). Thus, the outflow particles observed during SCOUT-AMMA show

ACPD
11, 745–812, 2011

more complex shapes than the former SVC particle observations, which is in good qualitative agreement with the MAS observations.

Two cases of New Particle Formation events were encountered on 7 and 11 August inside of ice clouds close to or in an MCS outflow. While during the event of 11 August the ice particle number concentrations were low, the case of 7 August showed that the NPF event is quenched when ice particle numbers increase. This agrees with observations by Weigel et al. (2011). The NPF event on 11 August showed an interesting feature when approaching the air mass boundary between outflow air and upper tropospheric background air. Here, the NPF peaks with a very high amount of newly formed particles, possibly due to entrainment and isobaric mixing of those two air masses.

By comparing total aerosol number concentrations to ice particle concentrations estimations of the interstitial aerosol and the activation ratio is given. The separation of deep convective events, SVC events, and NPF events yields a significant difference in the activation ratios. While for the deep convective cases (MCS outflow and convective overshooting as observed during the SCOUT-O3 campaign, see De Reus et al., 2009) one cloud particle occurs roughly per 1000 aerosol particles, in some cases even per 300 aerosol particles, the SVC show just one or even less cloud particles per 30 000 aerosol particles. This is in agreement to Jensen et al. (2010) who state that only few aerosol particles will act as very efficient ice nuclei in the formation of SVC. NPF events seem to prefer circumstances where only few cloud particles are present.

We would like to emphasise that high quality in-situ measurements in the tropical UT/LS are difficult to obtain since specialised high altitude research aircraft and instrumentation are required in this challenging environment. Thus, also the data set of such observations is small and to provide useful parameterisations of either MCS outflow clouds or SVC including microphysical parameters more measurements are needed.

Acknowledgements. The SCOUT-O3 and SCOUT-AMMA projects were funded by the European Commission through Contract 505390-GOCE-CT-2004-505390 and the EC Integrated Projects AMMA-EU (Contract no. 004089-2). The M55 "Geophysica" campaign was supported

ACPD
11, 745–812, 2011

by the EEIG-Geophysica Consortium, CNRS-INSU, CNES, and EUFAR. The DLR Falcon-20 campaigns were funded through TROCCINOX, SCOUT-O3, AMMA-EU, and DLR.

Based on a French initiative, AMMA was built by an international scientific group and funded by a large number of agencies, especially from France, the UK, the United States, Africa, and – for us – German sources. It has been a beneficiary of a major financial contribution from the European Community Sixth Framework Programme (AMMA-EU). Significant financial support for our activities with the M-55 "Geophysica" in Australia and Burkina Faso also was supplied by the Max Planck Society.

For the CIP data processing we gratefully acknowledge help from Aaron Bansemer (NCAR, Boulder, Co, USA). For very helpful comments on the manuscript we thank Jasmine Cetrone from the University of Washington, Seattle, USA. We thank Stefano Balestri, Ana Alfaro Martinez (ERS), and the pilots, engineers, crew of the M-55 "Geophysica". The local authorities, scientists and staff in Ouagadougou (Burkina Faso) were wonderful hosts, and we thank for their amazing hospitality and support during this in many respects challenging campaign in Burkina Faso, which for all of us was a deeply moving life experience. Special thanks are due to Toro Drabo from the University in Ouagadougou.

The service charges for this open access publication
have been covered by the Max Planck Society.

References

Ackerman, T. P., Liou, K. N., Valero, F. P. J., and Pfister, L.: Heating rates in tropical anvils, J. Atmos. Sci., 45, 1606–1623, 1988. 748

Baker, B. and Lawson, R. P.: Improvement in determination of ice water content from two-dimensional particle imagery. Part I: Image-to-mass relationships, J. Appl. Meteorol. Clim., 45, 1282–1290, 2006. 755

Barnes, G.: Severe Convective Storms, vol. 28 of AMS Meteorological Monograph Series, chap. 10: Severe local storms in the tropics, AMS, 358–432, 2001. 748, 749

Barret, B., Williams, J. E., Bouarar, I., Yang, X., Josse, B., Law, K., Pham, M., Le Flochmoën, E., Liousse, C., Peuch, V. H., Carver, G. D., Pyle, J. A., Sauvage, B., van Velthoven, P., Schlager, H., Mari, C., and Cammas, J.-P.: Impact of West African Monsoon convective transport and lightning NO_x production upon the upper tropospheric composition: a multi-model study, Atmos. Chem. Phys., 10, 5719–5738, doi:10.5194/acp-10-5719-2010, 2010. 749, 768

Barth, M. C., Stuart, A. L., and Skamarock, W. C.: Numerical simulations of the July 10, 1996, Stratospheric-Tropospheric Experiment: Radiation, Aerosols, and Ozone (STERAO)-Deep Convection experiment storm: Redistribution of soluble tracers, J. Geophys. Res.-Atmos., 106, 12381–12400, 2001. 750

Barth, M. C., Kim, S.-W., Wang, C., Pickering, K. E., Ott, L. E., Stenchikov, G., Leriche, M., Cautenet, S., Pinty, J.-P., Barthe, Ch., Mari, C., Helsdon, J. H., Farley, R. D., Fridlind, A. M., Ackerman, A. S., Spiridonov, V., and Telenta, B.: Cloud-scale model intercomparison of chemical constituent transport in deep convection, Atmos. Chem. Phys., 7, 4709–4731, doi:10.5194/acp-7-4709-2007, 2007. 750

Baumgardner, D., Dye, J. E., Gandrud, B. W., and Knollenberg, R. G.: Interpretation of measurements made by the forward scattering spectrometer probe (Fssp-300) during the airborne arctic stratospheric expedition, J. Geophys. Res.-Atmos., 97, 8035–8046, 1992. 755

Borrmann, S., Luo, B. P., and Mishchenko, M.: Application of the T-matrix method to the measurement of aspherical (ellipsoidal) particles with forward scattering optical particle counters, J. Aerosol Sci., 31, 789–799, 2000. 770

Borrmann, S., Kunkel, D., Weigel, R., Minikin, A., Deshler, T., Wilson, J. C., Curtius, J., Volk, C. M., Homan, C. D., Ulanovsky, A., Ravegnani, F., Viciani, S., Shur, G. N., Belyaev, G. V., Law, K. S., and Cairo, F.: Aerosols in the tropical and subtropical UT/LS: in-situ measurements of submicron particle abundance and volatility, Atmos. Chem. Phys., 10, 5573–5592, doi:10.5194/acp-10-5573-2010, 2010. 750, 757

Brunner, D., Siegmund, P., May, P. T., Chappel, L., Schiller, C., Müller, R., Peter, T., Fueglistaler, S., MacKenzie, A. R., Fix, A., Schlager, H., Allen, G., Fjaeraa, A. M., Streibel, M., and Harris, N. R. P.: The SCOUT-O3 Darwin Aircraft Campaign: rationale and meteorology, Atmos. Chem. Phys., 9, 93–117, doi:10.5194/acp-9-93-2009, 2009. 756

Buontempo, C., Cairo, F., Di Donfrancesco, G., Morbidini, R., Viterbini, M., and Adriani, A.: Optical measurements of atmospheric particles from airborne platforms: in situ and remote sensing instruments for balloons and aircrafts, Ann. Geophys., 49, 57–64, 2006, http://www.ann-geophys.net/49/57/2006/. 758

Cairo, F., Adriani, A., Viterbini, M., Di Donfrancesco, G., Mitev, V., Matthey, R., Bastiano, M., Redaelli, G., Dragani, R., Ferretti, R., Rizi, V., Paolucci, T., Bernardini, L., Cacciani, M.,

Discussion Paper | Discussion Paper | Discussion Paper | Discussion Paper |

ACPD

11, 745–812, 2011

Tropical ice clouds: MCS outflow, anvil, and subvisual cirrus

W. Frey et al.

Pace, G., and Fiocco, G.: Polar stratospheric clouds observed during the Airborne Polar Experiment-Geophysica Aircraft in Antarctica (APE-GAIA) campaign, J. Geophys. Res., 109, D07204, doi:10.1029/2003JD003930, 2004. 758

Cairo, F., Di Donfrancesco, G., Snels, M., Fierli, F., Viterbini, M., Borrmann, S., and Frey, W.: A comparison of light backscattering and particle size distribution measurements in tropical cirrus clouds, Atmos. Meas. Tech. Discuss., 3, 4059–4089, doi:10.5194/amtd-3-4059-2010, 2010a. 756

Cairo, F., Pommereau, J. P., Law, K. S., Schlager, H., Garnier, A., Fierli, F., Ern, M., Streibel, M., Arabas, S., Borrmann, S., Berthelier, J. J., Blom, C., Christensen, T., D'Amato, F., Di Donfrancesco, G., Deshler, T., Diedhiou, A., Durry, G., Engelsen, O., Goutail, F., Harris, N. R. P., Kerstel, E. R. T., Khaykin, S., Konopka, P., Kylling, A., Larsen, N., Lebel, T., Liu, X., MacKenzie, A. R., Nielsen, J., Oulanowski, A., Parker, D. J., Pelon, J., Polcher, J., Pyle, J. A., Ravegnani, F., Rivière, E. D., Robinson, A. D., Röckmann, T., Schiller, C., Simões, F., Stefanutti, L., Stroh, F., Some, L., Siegmund, P., Sitnikov, N., Vernier, J. P., Volk, C. M., Voigt, C., von Hobe, M., Viciani, S., and Yushkov, V.: An introduction to the SCOUT-AMMA stratospheric aircraft, balloons and sondes campaign in West Africa, August 2006: rationale and roadmap, Atmos. Chem. Phys., 10, 2237–2256, doi:10.5194/acp-10-2237-2010, 2010b. 753, 758

Cetrone, J. and Houze, R. A.: Anvil clouds of tropical mesoscale convective systems in monsoon regions, Q. J. Roy. Meteor. Soc., 135, 305–317, 2009. 749, 761, 775

Chong, M.: The 11 August 2006 squall-line system as observed from MIT Doppler radar during the AMMA SOP, Q. J. Roy. Meteor. Soc., 136, 209–226, doi:10.1002/qj.466, 2010. 764

Corti, T., Luo, B. P., Fu, Q., Vömel, H., and Peter, T.: The impact of cirrus clouds on tropical troposphere-to-stratosphere transport, Atmos. Chem. Phys., 6, 2539–2547, doi:10.5194/acp-6-2539-2006, 2006. 753

Corti, T., Luo, B. P., de Reus, M., Brunner, D., Cairo, F., Mahoney, M. J., Martucci, G., Matthey, R., Mitev, V., dos Santos, F. H., Schiller, C., Shur, G., Sitnikov, N. M., Spelten, N., Vössing, H. J., Borrmann, S., and Peter, T.: Unprecedented evidence for deep convection hydrating the tropical stratosphere, Geophys. Res. Lett., 35, L10810, doi:10.1029/2008GL033641, 2008. 749

Curtius, J., Weigel, R., Vössing, H.-J., Wernli, H., Werner, A., Volk, C.-M., Konopka, P., Krebsbach, M., Schiller, C., Roiger, A., Schlager, H., Dreiling, V., and Borrmann, S.: Observations of meteoric material and implications for aerosol nucleation in the winter Arctic lower stratosphere derived from in situ particle measurements, Atmos. Chem. Phys., 5, 3053–3069, doi:10.5194/acp-5-3053-2005, 2005. 757, 765

Cziczo, D. J., Stetzer, O., Worringen, A., Ebert, M., Weinbruch, S., Kamphus, M., Gallavardin, S. J., Curtius, J., Borrmann, S., Froyd, K. D., Mertes, S., Möhler, O., and Lohmann, U.: Inadvertent climate modification due to anthropogenic lead, Nat. Geosci., 2, 333–336, 2009. 751

Davis, S., Hlavka, D., Jensen, E., Rosenlof, K., Yang, Q., Schmidt, S., Borrmann, S., Frey, W., Lawson, P., Voemel, H., and Bui, T. P.: In situ and lidar observations of tropopause subvisible cirrus clouds during TC4, J. Geophys. Res.-Atmos., 115, D00J17, doi:10.1029/2009JD013093, 2010. 748, 750, 752, 769, 770, 776, 810

de Reus, M., Borrmann, S., Bansemer, A., Heymsfield, A. J., Weigel, R., Schiller, C., Mitev, V., Frey, W., Kunkel, D., Kürten, A., Curtius, J., Sitnikov, N. M., Ulanovsky, A., and Ravegnani, F.: Evidence for ice particles in the tropical stratosphere from in-situ measurements, Atmos. Chem. Phys., 9, 6775–6792, doi:10.5194/acp-9-6775-2009, 2009. 749, 754, 755, 757, 760, 762, 773, 774, 777, 790, 794

DeMott, P. J., Sassen, K., Poellot, M. R., Baumgardner, D., Rogers, D. C., Brooks, S. D., Prenni, A. J., and Kreidenweis, S. M.: African dust aerosols as atmospheric ice nuclei, Geophys. Res. Lett., 30, 1732, 2003. 751

Field, P. R., Heymsfield, A. J., and Bansemer, A.: Shattering and particle interarrival times measured by optical array probes in ice clouds, J. Atmos. Ocean. Tech., 23, 1357–1371, 2006. 755, 756, 790

Fierli, F., Orlandi, E., Law, K. S., Cagnazzo, C., Cairo, F., Schiller, C., Borrmann, S., Didonfrancesco, G., Ravegnani, F., and Volk, M.: Impact of deep convection in the tropical tropopause layer in West Africa: in-situ observations and mesoscale modelling, Atmos. Chem. Phys. Discuss., 10, 4927–4961, doi:10.5194/acpd-10-4927-2010, 2010. 749, 754, 762

Fritsch, J. M. and Forbes, G. S.: Severe Convective Storms, vol. 28 of AMS Meteorological Monograph Series, chap. 9: Mesoscale Convective Systems, AMS, 323–357, 2001. 748

Froyd, K. D., Murphy, D. M., Sanford, T. J., Thomson, D. S., Wilson, J. C., Pfister, L., and Lait, L.: Aerosol composition of the tropical upper troposphere, Atmos. Chem. Phys., 9, 4363–4385, doi:10.5194/acp-9-4363-2009, 2009. 751

Froyd, K. D., Murphy, D. M., Lawson, P., Baumgardner, D., and Herman, R. L.: Aerosols that form subvisible cirrus at the tropical tropopause, Atmos. Chem. Phys., 10, 209–218,

ACPD

11, 745–812, 2011

doi:10.5194/acp-10-209-2010, 2010. 750, 751

Fueglistaler, S., Dessler, A. E., Dunkerton, T. J., Folkins, I., Fu, Q., and Mote, P. W.: Tropical tropopause layer, Rev. Geophys., 47, RG1004, doi:10.1029/2008RG000267, 2009. 749

Haag, W. and Kärcher, B.: The impact of aerosols and gravity waves on cirrus clouds at mid-latitudes, J. Geophys. Res.-Atmos., 109, D12202, doi:10.1029/2004JD004579, 2004. 752

Hall, N. M. J. and Peyrille, P.: Dynamics of the West African monsoon, J. Phys. IV, 139, 81–99, doi:10.1051/jp4:2006139007, 2006. 775

Heymsfield, A. J.: Ice particles observed in a cirriform cloud at −83 °C and implications for polar stratospheric clouds, J. Atmos. Sci., 43, 851–855, 1986. 769, 776

Heymsfield, A. J. and Parrish, J. L.: A computational technique for increasing the effective sampling volume of the PMS two-dimensional particle size spectrometer, J. Appl. Meteorol., 17, 1566–1572, 1978. 790

Heymsfield, A. J., Lewis, S., Bansemer, A., Iaquinta, J., Miloshevich, L. M., Kajikawa, M., Twohy, C., and Poellot, M. R.: A general approach for deriving the properties of cirrus and stratiform ice cloud particles, J. Atmos. Sci., 59, 3–29, 2002. 755

Homan, C. D., Volk, C. M., Kuhn, A. C., Werner, A., Baehr, J., Viciani, S., Ulanovski, A., and Ravegnani, F.: Tracer measurements in the tropical tropopause layer during the AMMA/SCOUT-O3 aircraft campaign, Atmos. Chem. Phys., 10, 3615–3627, doi:10.5194/acp-10-3615-2010, 2010. 749, 750, 754, 758

Houze, R. A.: Mesoscale convective systems, Rev. Geophys., 42, RG4003, doi:10.1029/2004RG000150, 2004. 748

Houze, R. A.: Observed structure of mesoscale convective systems and implications for large-scale heating, Q. J. Roy. Meteor. Soc., 115, 425–461, 1989. 776

Huntrieser, H., Schlager, H., Roiger, A., Lichtenstern, M., Schumann, U., Kurz, C., Brunner, D., Schwierz, C., Richter, A., and Stohl, A.: Lightning-produced NO_x over Brazil during TROCCINOX: airborne measurements in tropical and subtropical thunderstorms and the importance of mesoscale convective systems, Atmos. Chem. Phys., 7, 2987–3013, doi:10.5194/acp-7-2987-2007, 2007. 756

Huntrieser, H., Schlager, H., Lichtenstern, M., Roiger, A., Stock, P., Minikin, A., Höller, H., Schmidt, K., Betz, H.-D., Allen, G., Viciani, S., Ulanovsky, A., Ravegnani, F., and Brunner, D.: NO_x production by lightning in Hector: first airborne measurements during SCOUT-O3/ACTIVE, Atmos. Chem. Phys., 9, 8377–8412, doi:10.5194/acp-9-8377-2009, 2009. 749, 750

Jensen, E. J., Toon, O. B., Selkirk, H. B., Spinhirne, J. D., and Schoeberl, M. R.: On the formation and persistence of subvisible cirrus clouds near the tropical tropopause, J. Geophys. Res., 101, 21361–21375, doi:10.1029/95JD03575, 1996. 751

Jensen, E. J., Pfister, L., Ackerman, A. S., Tabazadeh, A., and Toon, O. B.: A conceptual model of the dehydration of air due to freeze-drying by optically thin, laminar cirrus rising slowly across the tropical tropopause, J. Geophys. Res.-Atmos., 106, 17237–17252, 2001. 751, 752

Jensen, E. J., Pfister, L., Bui, T. V., Lawson, P., Baker, B., Mo, Q., Baumgardner, D., Weinstock, E. M., Smith, J. B., Moyer, E. J., Hanisco, T. F., Sayres, D. S., Clair, J. M. St., Alexander, M. J., Toon, O. B., and Smith, J. A.: Formation of large (≃100 µm) ice crystals near the tropical tropopause, Atmos. Chem. Phys., 8, 1621–1633, doi:10.5194/acp-8-1621-2008, 2008. 751

Jensen, E. J., Lawson, P., Baker, B., Pilson, B., Mo, Q., Heymsfield, A. J., Bansemer, A., Bui, T. P., McGill, M., Hlavka, D., Heymsfield, G., Platnick, S., Arnold, G. T., and Tanelli, S.: On the importance of small ice crystals in tropical anvil cirrus, Atmos. Chem. Phys., 9, 5519–5537, doi:10.5194/acp-9-5519-2009, 2009. 755

Jensen, E. J., Pfister, L., Bui, T.-P., Lawson, P., and Baumgardner, D.: Ice nucleation and cloud microphysical properties in tropical tropopause layer cirrus, Atmos. Chem. Phys., 10, 1369–1384, doi:10.5194/acp-10-1369-2010, 2010. 752, 773, 777

Kärcher, B.: Properties of subvisible cirrus clouds formed by homogeneous freezing, Atmos. Chem. Phys., 2, 161–170, doi:10.5194/acp-2-161-2002, 2002. 751

Kärcher, B.: Cirrus clouds in the tropical tropopause layer: Role of heterogeneous ice nuclei, Geophys. Res. Lett., 31, L12101, doi:10.1029/2004GL019774, 2004. 751

Khaykin, S., Pommereau, J.-P., Korshunov, L., Yushkov, V., Nielsen, J., Larsen, N., Christensen, T., Garnier, A., Lukyanov, A., and Williams, E.: Hydration of the lower stratosphere by ice crystal geysers over land convective systems, Atmos. Chem. Phys., 9, 2275–2287, doi:10.5194/acp-9-2275-2009, 2009. 749, 754, 759

Khosrawi, F. and Konopka, P.: Enhanced particle formation and growth due to mixing processes in the tropopause region, Atmos. Environ., 37, 903–910, doi:10.1016/S1352-2310(02)00976-7, 2003. 766

Korolev, A.: Reconstruction of the sizes of spherical particles from their shadow images. Part I: Theoretical considerations, J. Atmos. Ocean. Tech., 24, 376–389, 2007. 790

Krämer, M., Schiller, C., Afchine, A., Bauer, R., Gensch, I., Mangold, A., Schlicht, S., Spelten,

ACPD
11, 745–812, 2011

Tropical ice clouds: MCS outflow, anvil, and subvisual cirrus

W. Frey et al.

N., Sitnikov, N., Borrmann, S., de Reus, M., and Spichtinger, P.: Ice supersaturations and cirrus cloud crystal numbers, Atmos. Chem. Phys., 9, 3505–3522, doi:10.5194/acp-9-3505-2009, 2009. 759

Krüger, K., Tegtmeier, S., and Rex, M.: Variability of residence time in the Tropical Tropopause Layer during Northern Hemisphere winter, Atmos. Chem. Phys., 9, 6717–6725, doi:10.5194/acp-9-6717-2009, 2009. 750

Kulkarni, G. and Dobbie, S.: Ice nucleation properties of mineral dust particles: determination of onset RH_i, IN active fraction, nucleation time-lag, and the effect of active sites on contact angles, Atmos. Chem. Phys., 10, 95–105, doi:10.5194/acp-10-95-2010, 2010. 751

Laing, A. G. and Fritsch, J. M.: The global population of mesoscale convective complexes, Q. J. Roy. Meteor. Soc., 123, 389–405, 1997. 748

Law, K. S., Fierli, F., Cairo, F., Schlager, H., Borrmann, S., Streibel, M., Real, E., Kunkel, D., Schiller, C., Ravegnani, F., Ulanovsky, A., D'Amato, F., Viciani, S., and Volk, C. M.: Air mass origins influencing TTL chemical composition over West Africa during 2006 summer monsoon, Atmos. Chem. Phys., 10, 10753–10770, doi:10.5194/acp-10-10753-2010, 2010. 749, 750, 754

Lawson, R. P., Pilson, B., Baker, B., Mo, Q., Jensen, E., Pfister, L., and Bui, P.: Aircraft measurements of microphysical properties of subvisible cirrus in the tropical tropopause layer, Atmos. Chem. Phys., 8, 1609–1620, doi:10.5194/acp-8-1609-2008, 2008. 750, 752, 755, 769, 770, 772, 776

Lee, S. H., Wilson, J. C., Baumgardner, D., Herman, R. L., Weinstock, E. M., LaFleur, B. G., Kok, G., Anderson, B., Lawson, P., Baker, B., Strawa, A., Pittman, J. V., Reeves, J. M., and Bui, T. P.: New particle formation observed in the tropical/subtropical cirrus clouds, J. Geophys. Res.-Atmos., 109, D20209, doi:10.1029/2004JD005033, 2004. 750

Liu, L. and Mishchenko, M. I.: Constraints on PSC particle microphysics derived from lidar observations, J. Quant. Spectrosc. Ra., 70, 817–831, 2001. 768

Luo, B. P., Peter, T., Fueglistaler, S., Wernli, H., Wirth, M., Kiemle, C., Flentje, H., Yushkov, V. A., Khattatov, V., Rudakov, V., Thomas, A., Borrmann, S., Toci, G., Mazzinghi, P., Beuermann, J., Schiller, C., Cairo, F., Di Donfrancesco, G., Adriani, A., Volk, C. M., Strom, J., Noone, K., Mitev, V., MacKenzie, R. A., Carslaw, K. S., Trautmann, T., Santacesaria, V., and Stefanutti, L.: Dehydration potential of ultrathin clouds at the tropical tropopause, Geophys. Res. Lett., 30, 1557, 2003a. 751, 769

Luo, B. P., Peter, Th., Wernli, H., Fueglistaler, S., Wirth, M., Kiemle, C., Flentje, H., Yushkov,

ACPD

11, 745–812, 2011

Tropical ice clouds: MCS outflow, anvil, and subvisual cirrus

W. Frey et al.

V. A., Khattatov, V., Rudakov, V., Thomas, A., Borrmann, S., Toci, G., Mazzinghi, P., Beuermann, J., Schiller, C., Cairo, F., Di Don-Francesco, G., Adriani, A., Volk, C. M., Strom, J., Noone, K., Mitev, V., MacKenzie, R. A., Carslaw, K. S., Trautmann, T., Santacesaria, V., and Stefanutti, L.: Ultrathin Tropical Tropopause Clouds (UTTCs): II. Stabilization mechanisms, Atmos. Chem. Phys., 3, 1093–1100, doi:10.5194/acp-3-1093-2003, 2003. 752, 769, 772

Massie, S., Gettelman, A., Randel, W., and Baumgardner, D.: Distribution of tropical cirrus in relation to convection, J. Geophys. Res.-Atmos., 107, 4591, doi:10.1029/2001JD001293, 2002. 772

McFarquhar, G. M. and Heymsfield, A. J.: Parameterization of tropical cirrus ice crystal size distributions and implications for radiative transfer: results from CEPEX, J. Atmos. Sci., 54, 2187–2200, doi:10.1175/1520-0469(1997)054<2187:POTCIC>2.0.CO;2, 1997. 760, 794

McFarquhar, G. M. and Heymsfield, A. J.: The definition and significance of an effective radius for ice clouds, J. Atmos. Sci., 55, 2039–2052, 1998. 755

McFarquhar, G. M., Heymsfield, A. J., Spinhirne, J., and Hart, B.: Thin and subvisual tropopause tropical cirrus: observations and radiative impacts, J. Atmos. Sci., 57, 1841–1853, 2000. 750, 769, 772, 776

Murray, B. J., Wilson, T. W., Dobbie, S., Cui, Z., Al-Jumur, S. M. R. K., Möhler, O., Schnaiter, M., Wagner, R., Benz, S., Niemand, M., Saathoff, H., Ebert, V., Wagner, S., and Karcher, B.: Heterogeneous nucleation of ice particles on glassy aerosols under cirrus conditions, Nat. Geosci., 3, 233–237, doi:10.1038/ngeo817, 2010. 751

Park, S., Jiménez, R., Daube, B. C., Pfister, L., Conway, T. J., Gottlieb, E. W., Chow, V. Y., Curran, D. J., Matross, D. M., Bright, A., Atlas, E. L., Bui, T. P., Gao, R.-S., Twohy, C. H., and Wofsy, S. C.: The CO_2 tracer clock for the Tropical Tropopause Layer, Atmos. Chem. Phys., 7, 3989–4000, doi:10.5194/acp-7-3989-2007, 2007. 749

Peter, Th., Luo, B. P., Wirth, M., Kiemle, C., Flentje, H., Yushkov, V. A., Khattatov, V., Rudakov, V., Thomas, A., Borrmann, S., Toci, G., Mazzinghi, P., Beuermann, J., Schiller, C., Cairo, F., Di Donfrancesco, G., Adriani, A., Volk, C. M., Strom, J., Noone, K., Mitev, V., MacKenzie, R. A., Carslaw, K. S., Trautmann, T., Santacesaria, V., and Stefanutti, L.: Ultrathin Tropical Tropopause Clouds (UTTCs): I. Cloud morphology and occurrence, Atmos. Chem. Phys., 3, 1083–1091, doi:10.5194/acp-3-1083-2003, 2003. 751, 769

Pfister, L., Selkirk, H. B., Jensen, E. J., Schoeberl, M. R., Toon, O. B., Browell, E. V., Grant, W. B., Gary, B., Mahoney, M. J., Bui, T. V., and Hintsa, E.: Aircraft observations of thin cirrus clouds near the tropical tropopause, J. Geophys. Res.-Atmos., 106, 9765–9786,

2001. 772
Plöger, F., Konopka, P., Günther, G., Grooß, J. U., and Müller, R.: Impact of the vertical velocity scheme on modeling transport in the tropical tropopause layer, J. Geophys. Res.-Atmos., 115, D03301, doi:10.1029/2009JD012023, 2010. 750
Pommereau, J. P.: Troposphere-to-stratosphere transport in the tropics, CR Geosci., 342, 331–338, 2010. 748
Protat, A., Delanoë, J., Plana-Fattori, A., May, P. T., and O'Connor, E. J.: The statistical properties of tropical ice clouds generated by the West African and Australian monsoons, from ground-based radar-lidar observations, Q. J. Roy. Meteor. Soc., 136, 345–363, doi:10.1002/qj.490, 2010. 748
Real, E., Orlandi, E., Law, K. S., Fierli, F., Josset, D., Cairo, F., Schlager, H., Borrmann, S., Kunkel, D., Volk, C. M., McQuaid, J. B., Stewart, D. J., Lee, J., Lewis, A. C., Hopkins, J. R., Ravegnani, F., Ulanovski, A., and Liousse, C.: Cross-hemispheric transport of Central African biomass burning pollutants: implications for downwind ozone production, Atmos. Chem. Phys., 10, 3027–3046, doi:10.5194/acp-10-3027-2010, 2010. 754
Sassen, K., Wang, Z., and Liu, D.: Cirrus clouds and deep convection in the tropics: insights from CALIPSO and CloudSat, J. Geophys. Res., 114, D00H06, doi:10.1029/2009JD011916, 2009. 750
Schiller, C., Krämer, M., Afchine, A., Spelten, N., and Sitnikov, N.: Ice water content of Arctic, midlatitude, and tropical cirrus, J. Geophys. Res., 113, D24208, doi:10.1029/2008JD010342, 2008. 759
Schumacher, C., Houze, R., and Kraucunas, I.: The tropical dynamical response to latent heating estimates derived from the TRMM precipitation radar, J. Atmos. Sci., 61, 1341–1358, 2004. 748
Schumann, U. and Huntrieser, H.: The global lightning-induced nitrogen oxides source, Atmos. Chem. Phys., 7, 3823–3907, doi:10.5194/acp-7-3823-2007, 2007. 750
Seifert, M., Ström, J., Krejci, R., Minikin, A., Petzold, A., Gayet, J.-F., Schlager, H., Ziereis, H., Schumann, U., and Ovarlez, J.: Aerosol-cirrus interactions: a number based phenomenon at all?, Atmos. Chem. Phys., 4, 293–305, doi:10.5194/acp-4-293-2004, 2004. 774
Shur, G., Sitnikov, N., and Drynkov, A.: A mesoscale structure of meteorological fields in the tropopause layer and in the lower stratosphere over the southern tropics (Brazil), Russ. Meteorol. Hydrol., 32, 487–494, doi:10.3103/S106837390708002X, 2007. 759
Sitnikov, N. M., Yushkov, V. A., Afchine, A. A., Korshunov, L. I., Astakhov, V. I., Ulanovskii, A. E.,

ACPD
11, 745–812, 2011

Tropical ice clouds: MCS outflow, anvil, and subvisual cirrus

W. Frey et al.

Krämer, M., Mangold, A., Schiller, C., and Ravegnani, F.: The FLASH instrument for water vapor measurements on board the high-altitude airplane, Instrum. Exp. Tech., 50, 113–121, 2007. 759

Sokolov, L. and Lepuchov, B.: Protocol of interaction between Unit for Connection with Scientific Equipment (UCSE) and on-board scientific equipment of Geophysica aircraft (Second edition), Myasishchev Design Bureau (MDB), 1998. 759

Spichtinger, P. and Cziczo, D. J.: Impact of heterogeneous ice nuclei on homogeneous freezing events in cirrus clouds, J. Geophys. Res.-Atmos., 115, D14208, doi:10.1029/2009JD012168, 2010. 752

Stefanutti, L., Mackenzie, A. R., Santacesaria, V., Adriani, A., Balestri, S., Borrmann, S., Khattatov, V., Mazzinghi, P., Mitev, V., Rudakov, V., Schiller, C., Toci, G., Volk, C. M., Yushkov, V., Flentje, H., Kiemle, C., Redaelli, G., Carslaw, K. S., Noone, K., and Peter, T.: The APE-THESEO tropical campaign: An overview, J. Atmos. Chem., 48, 1–33, 2004. 752

Thomas, A., Borrmann, S., Kiemle, C., Cairo, F., Volk, M., Beuermann, J., Lepuchov, B., Santacesaria, V., Matthey, R., Rudakov, V., Yushkov, V., MacKenzie, A. R., and Stefanutti, L.: In situ measurements of background aerosol and subvisible cirrus in the tropical tropopause region, J. Geophys. Res., 107, 4763, doi:10.1029/2001JD001385, 2002. 748, 750, 752, 769, 770

Ulanovsky, A. E., Yushkov, V. A., Sitnikov, N. M., and Ravegnani, F.: The FOZAN-II fast-response chemiluminescent airborne ozone analyzer, Instrum. Exp. Tech., 44, 249–256, 2001. 759

Vaughan, G., Schiller, C., MacKenzie, A. R., Bower, K., Peter, T., Schlager, H., Harris, N. R. P., and May, P. T.: SCOUT-03/ACTIVE – High-altitude aircraft measurements around deep tropical convection, B. Am. Meteorol. Soc., 89, 647, 2008. 756

Viciani, S., D'Amato, F., Mazzinghi, P., Castagnoli, F., Toci, G., and Werle, P.: A cryogenically operated laser diode spectrometer for airborne measurement of stratospheric trace gases, Appl. Phys. B-Lasers O., 90, 581–592, 2008. 759

Voigt, C., Schlager, H., Luo, B. P., Dörnbrack, A., Roiger, A., Stock, P., Curtius, J., Vössing, H., Borrmann, S., Davies, S., Konopka, P., Schiller, C., Shur, G., and Peter, T.: Nitric Acid Trihydrate (NAT) formation at low NAT supersaturation in Polar Stratospheric Clouds (PSCs), Atmos. Chem. Phys., 5, 1371–1380, doi:10.5194/acp-5-1371-2005, 2005. 758

Voigt, C., Kärcher, B., Schlager, H., Schiller, C., Krämer, M., de Reus, M., Vössing, H., Borrmann, S., and Mitev, V.: In-situ observations and modeling of small nitric acid-containing ice crystals, Atmos. Chem. Phys., 7, 3373–3383, doi:10.5194/acp-7-3373-2007, 2007. 758

Voigt, C., Schlager, H., Roiger, A., Stenke, A., de Reus, M., Borrmann, S., Jensen, E., Schiller, C., Konopka, P., and Sitnikov, N.: Detection of reactive nitrogen containing particles in the tropopause region evidence for a tropical nitric acid trihydrate (NAT) belt, Atmos. Chem. Phys., 8, 7421–7430, doi:10.5194/acp-8-7421-2008, 2008. 758

Voigt, C., Schumann, U., Jurkat, T., Schäuble, D., Schlager, H., Petzold, A., Gayet, J.-F., Krämer, M., Schneider, J., Borrmann, S., Schmale, J., Jessberger, P., Hamburger, T., Lichtenstern, M., Scheibe, M., Gourbeyre, C., Meyer, J., Kübbeler, M., Frey, W., Kalesse, H., Butler, T., Lawrence, M. G., Holzäpfel, F., Arnold, F., Wendisch, M., Döpelheuer, A., Gottschaldt, K., Baumann, R., Zöger, M., Sölch, I., Rautenhaus, M., and Dörnbrack, A.: In-situ observations of young contrails – overview and selected results from the CONCERT campaign, Atmos. Chem. Phys., 10, 9039–9056, doi:10.5194/acp-10-9039-2010, 2010. 755

Volk, C. M., Riediger, O., Strunk, M., Schmidt, U., Ravegnani, F., Ulanovsky, A., and Rudakov, V.: In situ tracer measurements in the tropical tropopause region during APE-THESEO, in: Stratospheric Ozone 1999, Proc. 5th European Workshop on Stratospheric Ozone, edited by: Harris, N. R. P., Guirlet, M., and Amanatidis, G. T., no. 73 in EUR19340, St. Jean de Luz, 661–664, 2000. 758

Wang, P. K.: Moisture plumes above thunderstorm anvils and their contributions to cross-tropopause transport of water vapor in midlatitudes, J. Geophys. Res.-Atmos., 108, 4194, 2003. 753

Wang, P.-H., Minnis, P., McCormick, M. P., Kent, G. S., and Skeens, K. M.: A 6-year climatology of cloud occurrence frequency from Stratospheric Aerosol and Gas Experiment II observations (1985–1990), J. Geophys. Res., 101, 29407–29429, doi:10.1029/96JD01780, 1996. 750

Weigel, R., Hermann, M., Curtius, J., Voigt, C., Walter, S., Böttger, T., Lepukhov, B., Belyaev, G., and Borrmann, S.: Experimental characterization of the COndensation PArticle counting System for high altitude aircraft-borne application, Atmos. Meas. Tech., 2, 243–258, doi:10.5194/amt-2-243-2009, 2009. 757, 765

Weigel, R., Borrmann, S., Kazil, J., Stohl, A., Curtius, J., Minikin, A., Kunkel, D., de Reus, M., Frey, W., Lovejoy, E. R., Volk, C.-M., Cairo, F., and Law, K. S.: New particle formation in the tropical upper troposphere: in-situ measurements from South America and West Africa and the role of ion-induced nucleation, Atmos. Chem. Phys. Discuss., in preparation, 2011. 750, 758, 763, 774, 777

Winker, D. M. and Trepte, C. R.: Laminar cirrus observed near the tropical tropopause by LITE, Geophys. Res. Lett., 25, 3351–3354, 1998. 750, 751

Yushkov, V., Oulanovsky, A., Lechenuk, N., Roudakov, I., Arshinov, K., Tikhonov, F., Stefanutti, L., Ravegnani, F., Bonafe, U., and Georgiadis, T.: A Chemiluminescent Analyzer for Stratospheric Measurements of the Ozone Concentration (FOZAN), J. Atmos. Ocean. Tech., 16, 1345–1350, doi:10.1175/1520-0426(1999)016<1345:ACAFSM>2.0.CO;2, 1999. 759

Zimmermann, F., Weinbruch, S., Schütz, L., Hofmann, H., Ebert, M., Kandler, K., and Worringen, A.: Ice nucleation properties of the most abundant mineral dust phases, J. Geophys. Res.-Atmos., 113, D23204, doi:10.1029/2008JD010655, 2008. 751

Zipser, E. J., Cecil, D. J., Liu, C. T., Nesbitt, S. W., and Yorty, D. P.: Where are the most intense thunderstorms on earth?, B. Am. Meteorol. Soc., 87, 1057–1071, 2006. 748

Zöger, M., Afchine, A., Eicke, N., Gerhards, M.-T., Klein, E., McKenna, D. S., Mörschel, U., Schmidt, U., Tan, V., Tuitjer, F., Woyke, T., and Schiller, C.: Fast in situ stratospheric hygrometers: A new family of balloon-borne and airborne Lyman α photofragment fluorescence hygrometers, J. Geophys. Res., 104, 1807–1816, doi:10.1029/1998JD100025, 1999. 759

ACPD

11, 745–812, 2011

Table 1. Applied correction mechanisms for the CIP particle image analysis with the respective references.

reason for correction	description of solution	reference
first slice	reconstruction of lost first slice due to acquisition start-up time	De Reus et al. (2009)
area ratio	rejection of streakers and multiple particles in one image frame due to an area ratio below 0.1	De Reus et al. (2009)
out of focus	size and sample volume correction for out of focus particles that show a Poisson spot	Korolev (2007)
empty images	reconstruction as one pixel image	De Reus et al. (2009)
shattering	rejection of particles with interarrival time below a specific threshold which is chosen for each flight individually	Field et al. (2006)
partial images	reconstruction of images that touch an end diode (especially young outflow clouds contain large particles), reconstructed particles that exceed a size of 3000 µm (≈ twice the array width) are rejected (no complete rejection as in De Reus et al., 2009)	Heymsfield and Parrish (1978)

Discussion Paper | Discussion Paper | Discussion Paper | Discussion Paper |

ACPD

11, 745–812, 2011

Tropical ice clouds: MCS outflow, anvil, and subvisual cirrus

W. Frey et al.

ACPD

11, 745–812, 2011

Tropical ice clouds: MCS outflow, anvil, and subvisual cirrus

W. Frey et al.

Table 2. Parameters as defined in Eq. (1) for the two/three modal lognormal size distributions fitted to the median size distribution for each temperature bin as shown in Fig. 1.

$T_{potential}$ (K)	N (cm^{-3})	$\overline{D_p}$ (µm)	σ	Mode #
365–375	0.0036	6.6	1.5	1
	0.0017	15.3	1.23	2
355–365	0.013	9.5	1.7	1
	0.0025	40	1.4	2
345–355	0.25	9	1.7	1
	0.06	30	1.6	2
	0.018	170	1.6	3

Table 3. Measurement details substantiating the air mass change before and after the NPF peak in Fig. 9 between 58 310 s UTC and 58 350 s UTC on 11 August 2006.

	MCS outflow	UT background
Time (s UTC)	58 310	58 350
Altitude (km)	14.4	14.7
Pressure (hPa)	133	127.2
T (K)	201	200.5
$T_{potential}$ (K)	358	362
RHi (%)	80	38
$f_{non\ volatile}$ (%)	5.9	46
CO_2 (µmol/mol)	375	380

ACPD
11, 745–812, 2011

Table 4. Summary of the microphysical parameters of the four West African SVC cases in August 2006. The parameters include effective radius (r_{eff}), number concentrations for cloud particles (N_{cloud}, larger 2.7 µm) and aerosol particles ($N_{aerosol}$, larger 15 nm), aerosol volume backscatter coefficient (Ba), and aerosol depolarization ratio (Da)

	SVC1	SVC2	SVC3	SVC4
r_{eff} (µm)	2.3	20.9	20.4	5.8
IWC (g m^{-3})	0.3×10^{-5}	15×10^{-5}	38×10^{-5}	1.7×10^{-5}
N_{cloud} (cm^{-3})	2×10^{-3}	9×10^{-3}	24×10^{-3}	7×10^{-3}
$N_{aerosol}$ (cm^{-3})	408	479	776	302
RHi (%)	130	86	n.a.	94
T (K)	192	195	198	195
Ba (m^{-1} sr^{-1})	6.6×10^{-8}	1.3×10^{-7}	1.7×10^{-7}	1.1×10^{-7}
Da (%)	28	45	77	63

ACPD
11, 745–812, 2011

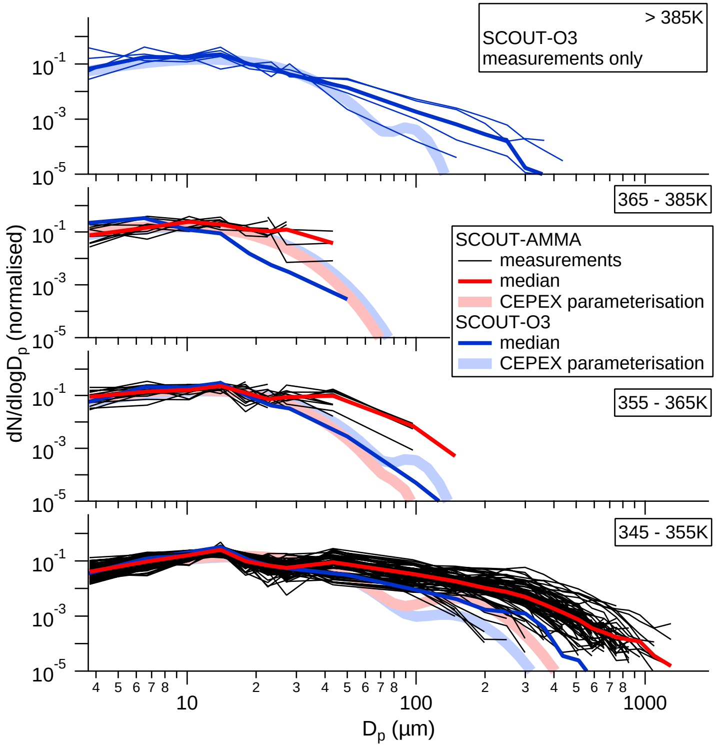

Fig. 1. Normalised ice particle size distributions of the cloud encounters during SCOUT-AMMA (black lines) in West Africa (2006): These M-55 "Geophysica" in-situ measurements are separated into four potential temperature bins with the median for each bin in bright red. The shaded pale red curves result from the CEPEX parameterisation after McFarquhar and Heymsfield (1997). For comparison M-55 "Geophysica" data from the Hector MCS in Northern Australia (during the 2005 SCOUT-O3 campaign) are shown with medians in bright blue and a corresponding CEPEX parameterisation in shaded pale blue (from De Reus et al., 2009).

ACPD
11, 745–812, 2011

Tropical ice clouds: MCS outflow, anvil, and subvisual cirrus

W. Frey et al.

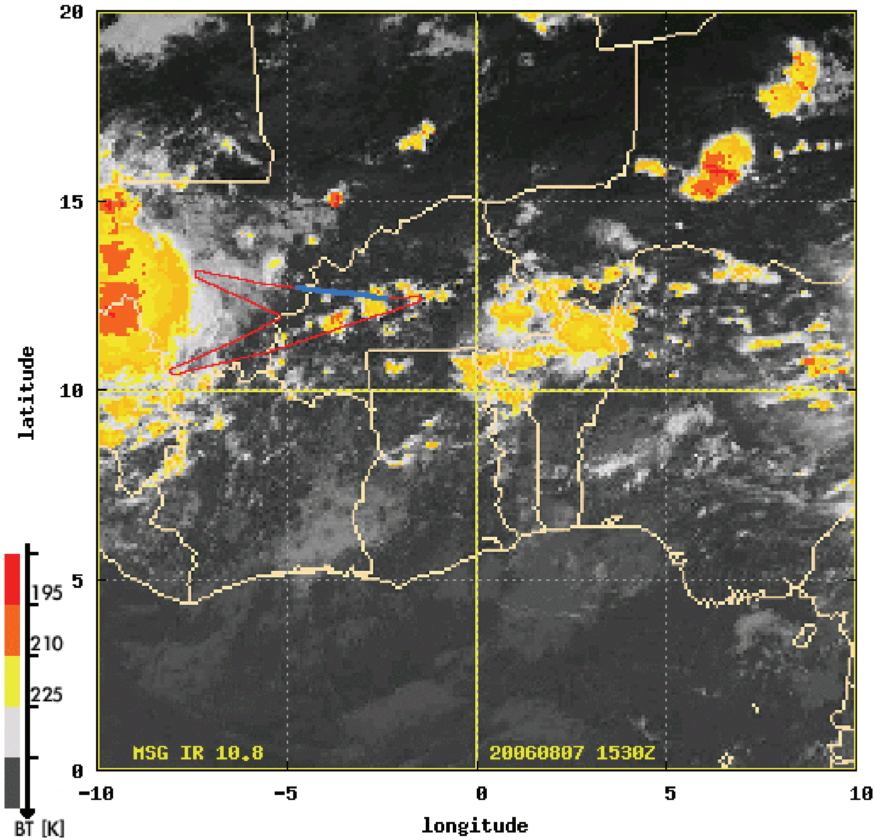

Fig. 2. Meteosat Second Generation (MSG) satellite image of Mesoscale Convective Systems (MCS) on 7 August 2006. The flight track of the M-55 "Geophysica" is indicated by the red/blue line. The blue part shows the flight segment of the time period for which the satellite image is valid and approximately where the measurements of Fig. 3 were performed.

ACPD
11, 745–812, 2011

Tropical ice clouds: MCS outflow, anvil, and subvisual cirrus

W. Frey et al.

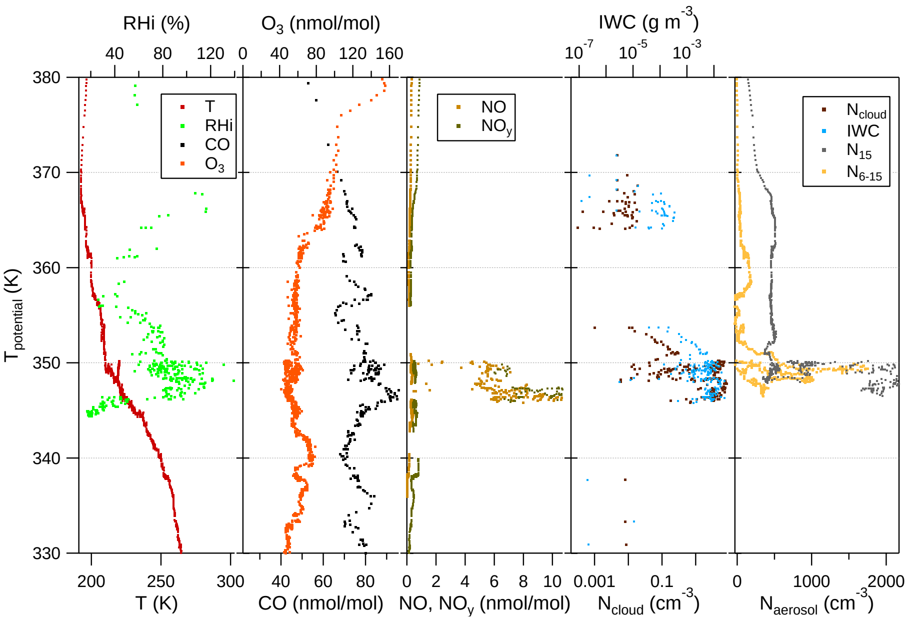

Fig. 3. Vertical profiles recorded by the instruments aboard M-55 "Geophysica" during its descent into Ouagadougou, Burkina Faso, on 7 August 2006.

ACPD
11, 745–812, 2011

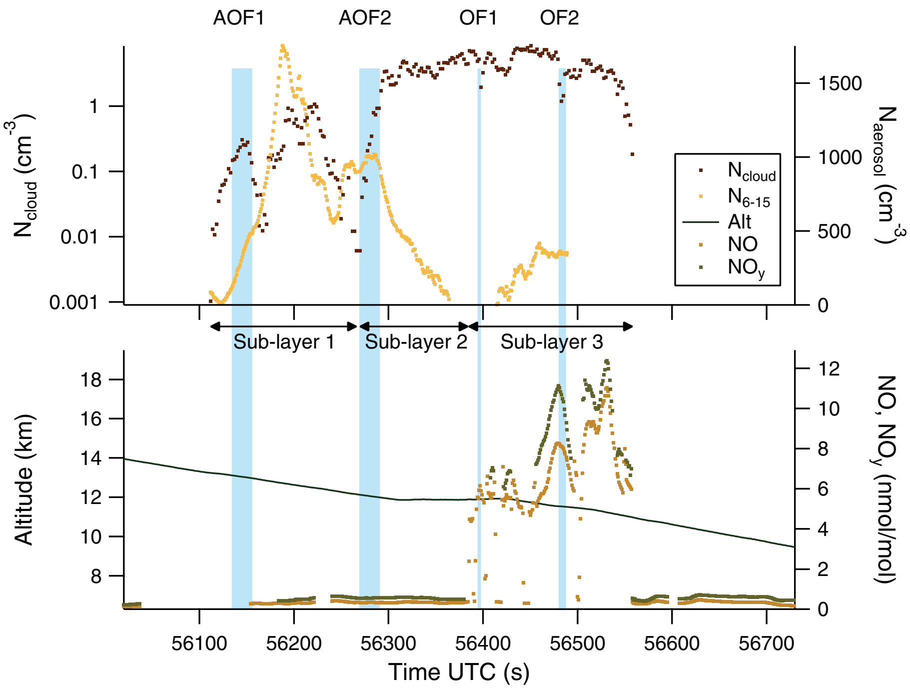

Fig. 4. Time series segment of the MCS anvil and outflow cloud crossing during descent on 7 August 2006. The shadings indicate time periods which were selected for deriving the ice particle size distributions as displayed in Fig. 5. ($N_{6–15}$ denotes the concentration difference $N_6 – N_{15}$.)

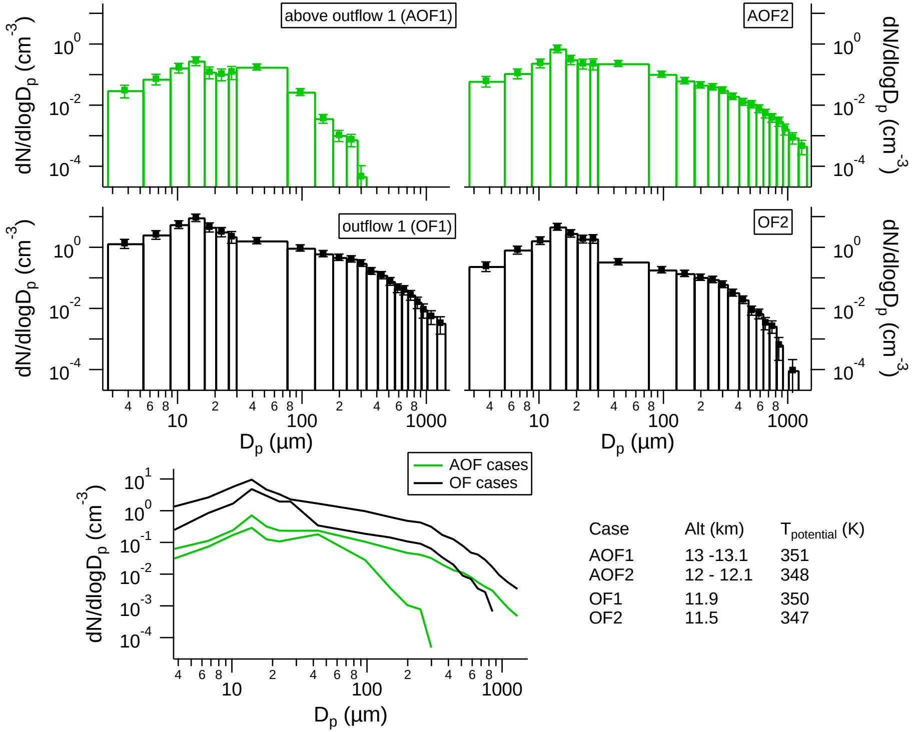

Fig. 5. Cloud particle size distributions with altitude information measured during the MCS anvil and outflow during descent on 7 August 2006 at the times and for the cases indicated in Fig. 4. The lowest panel summarises the ice particle size distributions of the four upper panels.

ACPD
11, 745–812, 2011

Tropical ice clouds: MCS outflow, anvil, and subvisual cirrus

W. Frey et al.

Title Page
Abstract | Introduction
Conclusions | References
Tables | Figures
◀| |▶
◀ ▶
Back | Close
Full Screen / Esc
Printer-friendly Version
Interactive Discussion

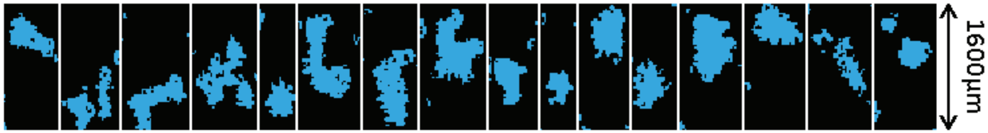

Fig. 6. Examples of cloud particle shadow-cast images collected by the CIP when crossing the MCS anvil and outflow while descending on 7 August 2006.

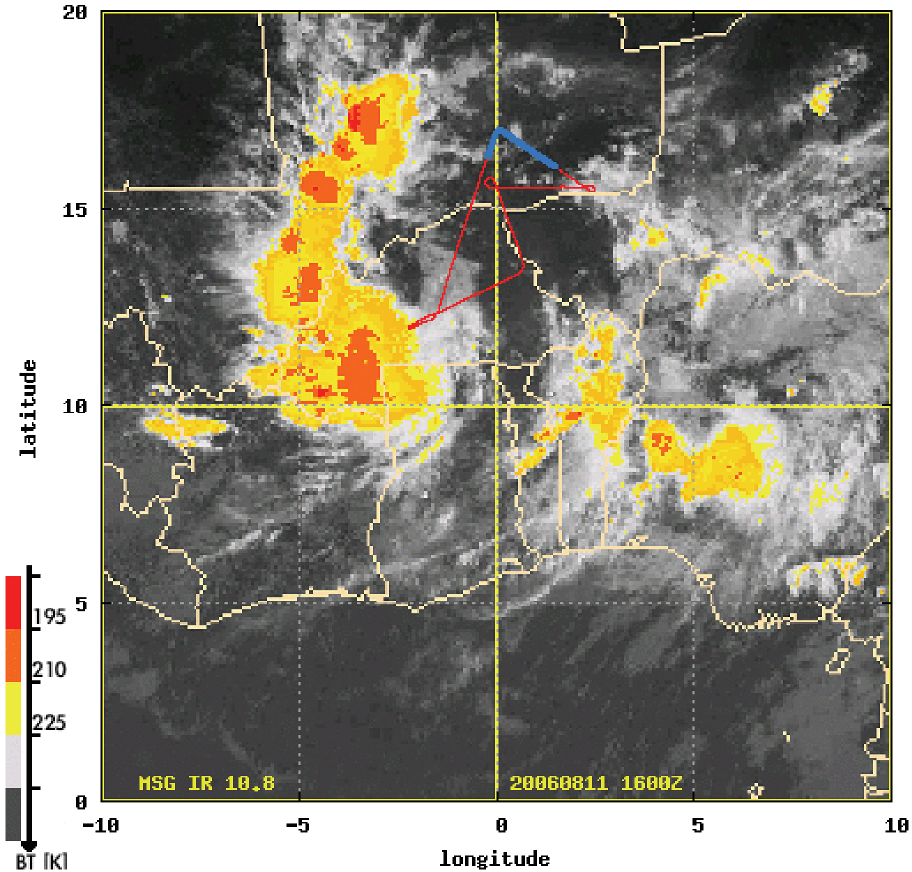

Fig. 7. MSG satellite image of the MCS on 11 August 2006 with the flight track of the M-55 “Geophysica” as indicated in blue/red.

ACPD
11, 745–812, 2011

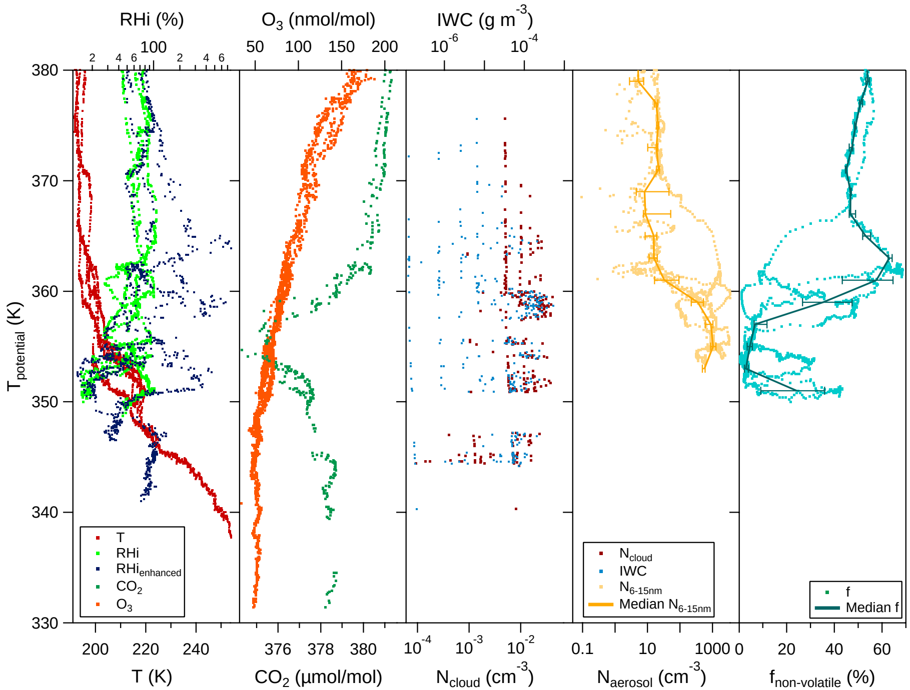

Fig. 8. Vertical profiles of the in-situ measurements from the M-55 "Geophysica" flight on 11 August 2006 during selected flight segments. The error bars in the two rightmost panels denote the 33 and 67 percentiles. The deviations within the measured parameters are a result of the fact that these measurements comprise several ascents/descents including dives within the flight.

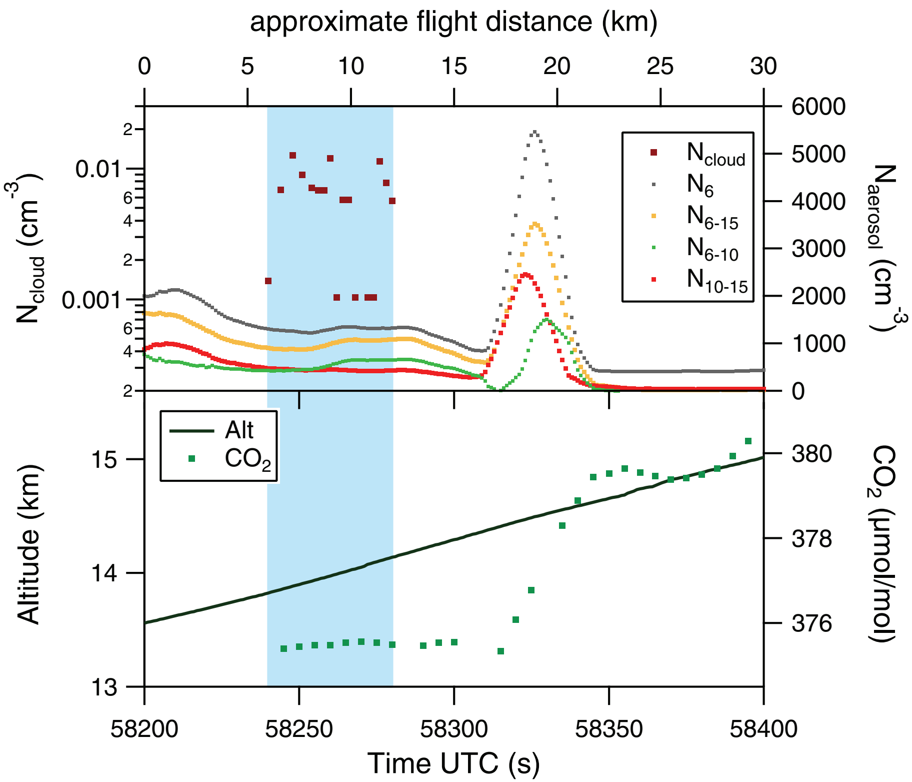

Fig. 9. Segment of the flight time series recorded on 11 August 2006. The blue shading indicates one of the aged outflow events encountered during this flight.

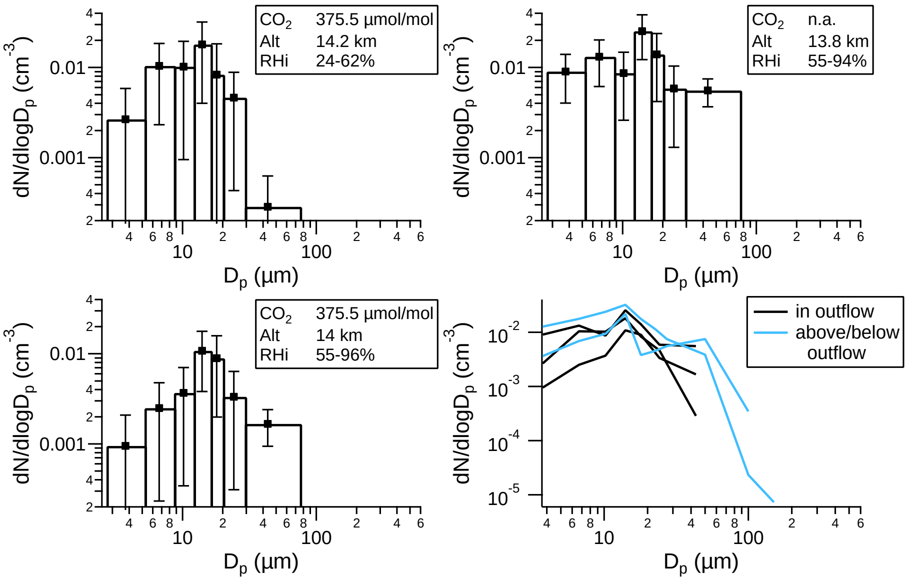

Fig. 10. Comparison of cloud particle size distributions from above, inside and below the aged outflow on 11 August 2006. The three black curves in the lower right panel show the single size distributions of the other panels for a better comparison along with one size distribution from a higher and one from a lower level than the outflow.

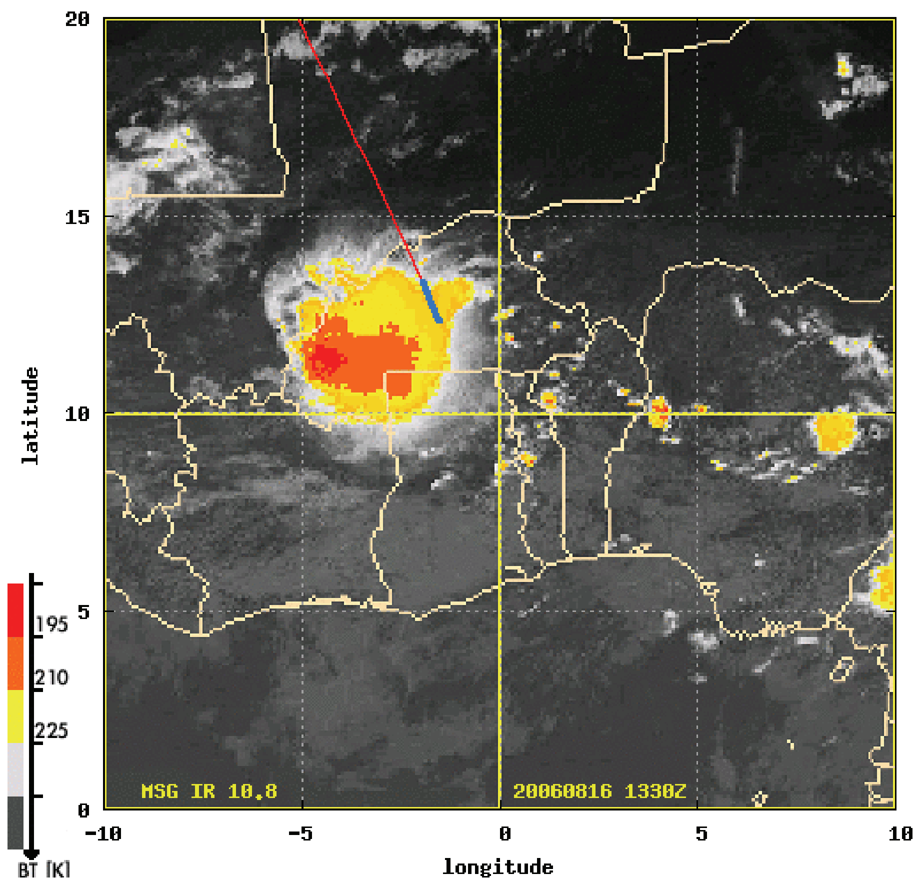

Fig. 11. MSG satellite image of the MCS on 16 August 2006 with the flight track of the M-55 "Geophysica" as indicated in blue/red.

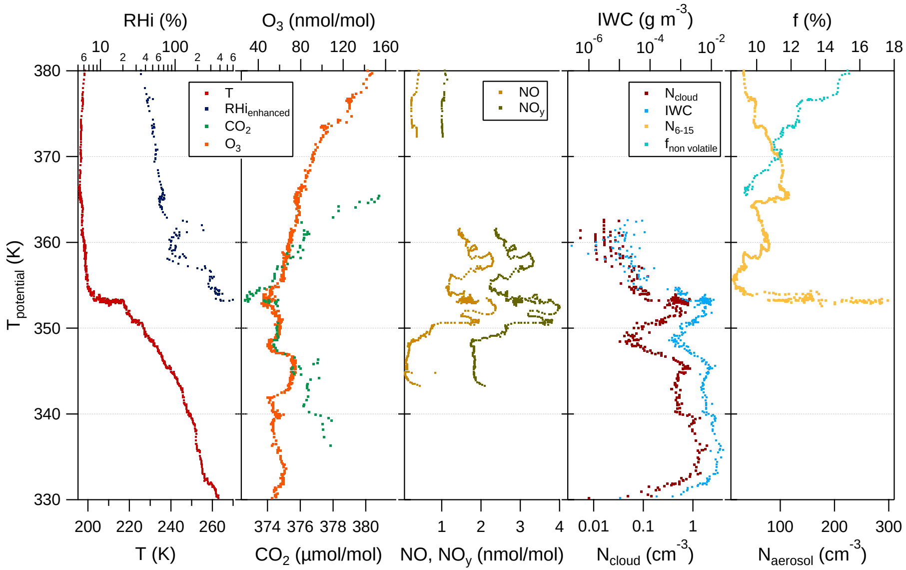

Fig. 12. Vertical profiles recorded by the M-55 "Geophysica" during its ascent from Ouagadougou, Burkina Faso, on 16 August 2006.

ACPD

11, 745–812, 2011

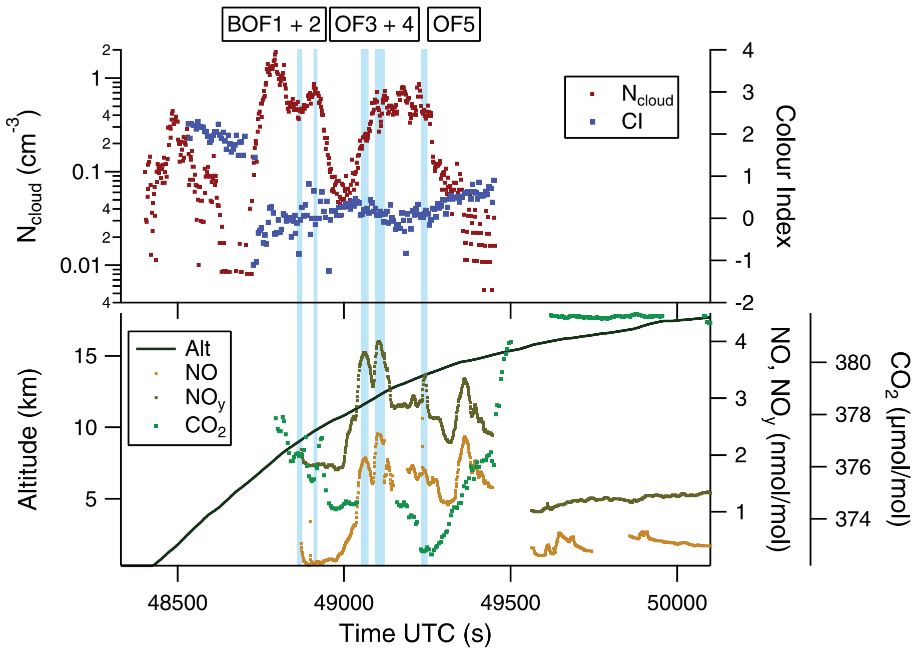

Fig. 13. Time series showing the ascent through the MCS anvil on 16 August 2006. The shading indicates time periods which were selected for deriving the ice particle size distributions from Fig. 14. (See text for details.)

ACPD
11, 745–812, 2011

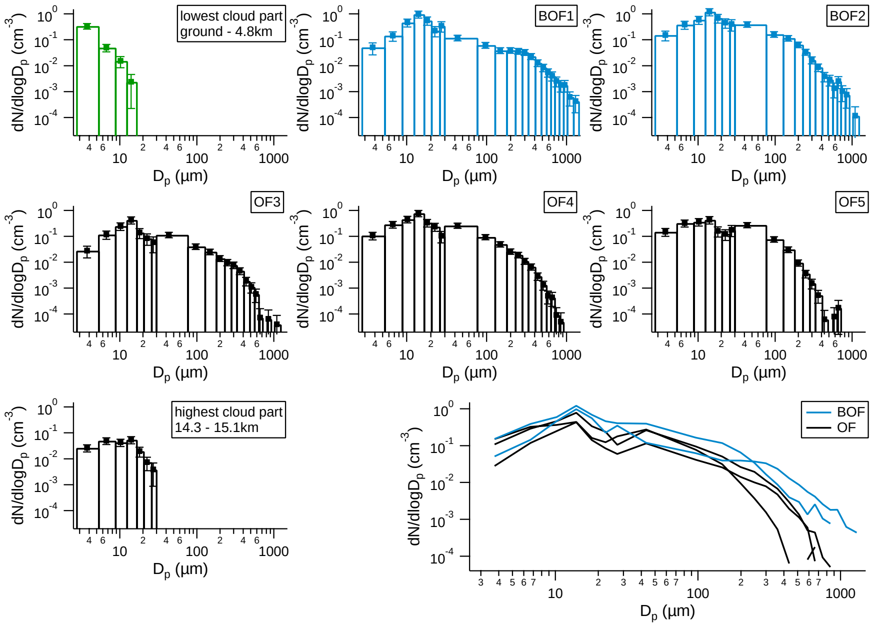

Case	$T_{potential}$ (K)	Alt (km)	O (nmol/mol)	NO_y (nmol/mol)	CO_2 (µmol/mol)
BOF1	343	9.0-9.1	a.	n.a.	376.5
BOF2	345	9.7-9.8	08-0.12	1.8	376.1
OF3	350-351	11.5-11.8	8-2	3.7-3.8	374.5
OF4	352-353	12.1-12.4	1-2.4	3.7-4	374.6
OF5	353-354	13.6-13.7	7-2.6	3-3.4	372.8

Fig. 14. Selected size distributions from the ascent on 16 August 2006 along with altitude and tracer mixing ratio information. The blue size distributions are compiled from measurements below the outflow (BOF1 and BOF2) and the black ones inside the outflow. The lower right panel summarises the ice particle size distributions from below and inside the outflow for comparison. The particle size distributions of the lowest and highest cloud parts are measured by the FSSP-100 only.

ACPD
11, 745–812, 2011

Tropical ice clouds: MCS outflow, anvil, and subvisual cirrus

W. Frey et al.

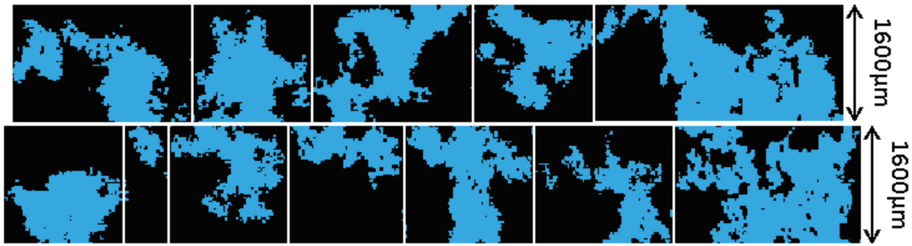

Fig. 15. Examples of CIP shadow images as observed at roughly 6 km altitude during the 16 August flight.

ACPD
11, 745–812, 2011

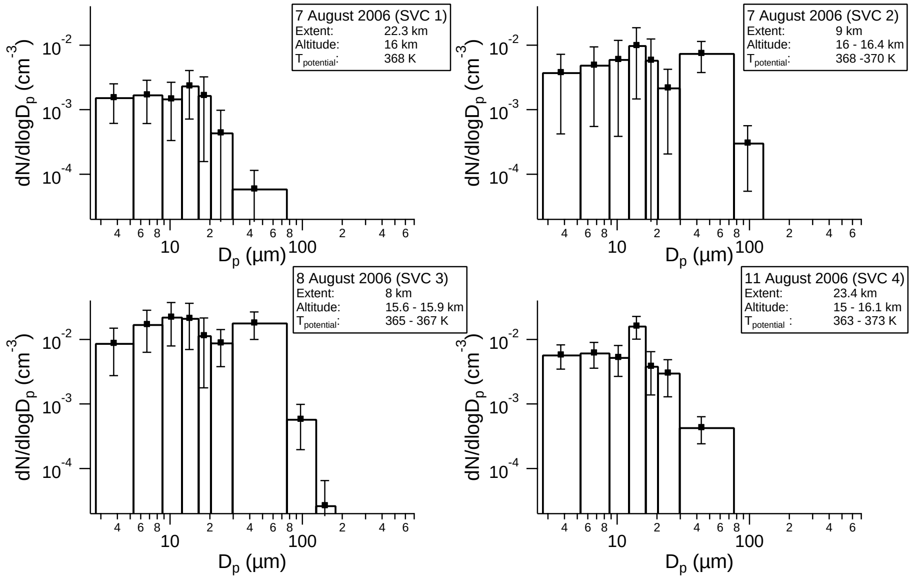

Fig. 16. Detailed subvisual cirrus (SVC) ice particle size distributions (combined FSSP-100 and CIP in-situ data) from 7, 8, and 11 August 2006 over West Africa. The horizontal extent (from flight time intervals), potential temperature levels, and altitudes of the cloud events SVC1 to SVC4 were as indicated in the boxes. The local cold point tropopause height was 16.3 km on 7 August 2006 and 16.5 km on the other days. The error bars result from uncertainties in the sampling volumes and counting statistics.

ACPD
11, 745–812, 2011

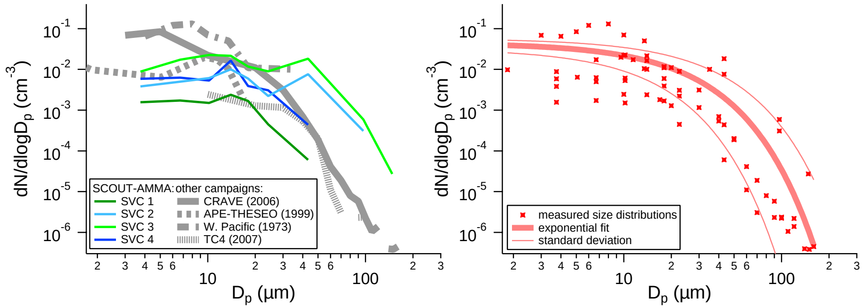

Fig. 17. Left panel (adapted from Davis et al., 2010): Overview of in-situ measurements for tropical SVC. The observations obtained during the indicated previous field experiments are shown in broad grey lines. The coloured lines depict the individual cloud encounters from SCOUT-AMMA in West Africa. Right panel: A parameterisation derived as exponential fit from all size distributions in the left panel with one sigma deviations. See Eq. (2) for the parameterisation and coefficients.

ACPD
11, 745–812, 2011

Title Page
Abstract | Introduction
Conclusions | References
Tables | Figures
◀| |▶
◀ ▶
Back | Close
Full Screen / Esc
Printer-friendly Version
Interactive Discussion

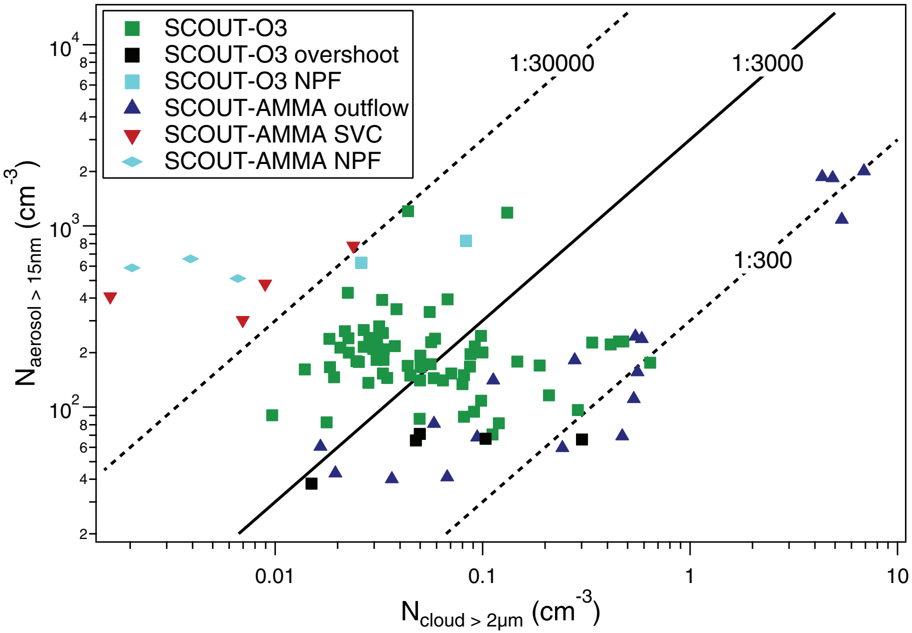

Fig. 18. Interstitial aerosol and cloud particle in-situ measurements of tropical cloud encounters in West-Africa (2006) and Northern Australia (2005). The ordinate shows the aerosol particle number concentration (measured by COPAS as proxy for the interstitial aerosol) covering size diameters between 15 nm and roughly 1 µm. The abscissa gives the simultaneously detected cloud particle number densities for sizes above 2 µm as measured by the CIP and FSSP-100 probes. The events are from the Australian Hector MCS (squares), the West African MCS outflows (blue triangles), and the West African SVCs (red triangles). Furthermore, NPF events are indicated in light blue. The lines indicate activation ratios in terms of the numbers of cloud particles and the available aerosol particles.

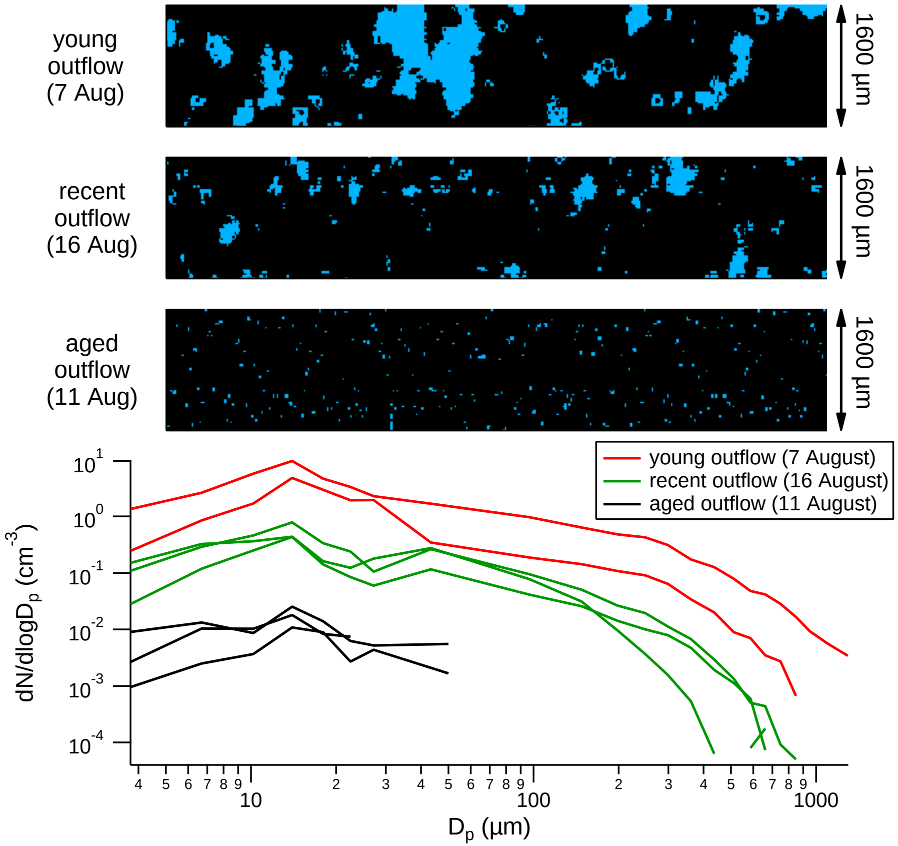

Fig. 19. Summary of outflow size distributions of the three flights on 7, 11, and 16 August 2006. Additionally, examples of consecutive CIP particle images for each outflow age are displayed on top starting with the youngest case.

ACPD
11, 745–812, 2011